

Rapid #: -21993448

CROSS REF ID: **693722**

LENDER: **CVM (California State Univ Maritime) :: Main Library**

BORROWER: **HDC (Claremont Colleges) :: Honnold Mudd Library**

TYPE: Article CC:CCG

JOURNAL TITLE: Applied thermal engineering

USER JOURNAL TITLE: APPLIED THERMAL ENGINEERING

ARTICLE TITLE: Review of daytime radiative cooling technologies and control methods

ARTICLE AUTHOR: Su, WG

VOLUME: 235

ISSUE:

MONTH:

YEAR: 2023

PAGES: unknown

ISSN: 1359-4311

OCLC #:

Processed by RapidX: 2/5/2024 10:36:22 AM

This material may be protected by copyright law (Title 17 U.S. Code)



Review of daytime radiative cooling technologies and control methods

Weiguang Su^{a,b,*}, Pei Cai^{a,b}, Jo Darkwa^c, Mingke Hu^d, Georgios Kokogiannakis^e, Chonghai Xu^{a,b}, Li Wang^{a,b}

^a School of Mechanical Engineering, Qilu University of Technology (Shandong Academy of Sciences), 250353 Jinan, China

^b Shandong Institute of Mechanical Design and Research, 250031 Jinan, China

^c Faculty of Engineering, University of Nottingham, University Park, Nottingham NG7 2RD, UK

^d Department of Mechanical Engineering, National University of Singapore, 9 Engineering Drive 1, Singapore 117542, Singapore

^e Sustainable Buildings Research Centre, University of Wollongong, NSW 2519, Wollongong, Australia



ARTICLE INFO

Keywords:

Daytime radiative cooler
Cooling performance
Manufacturing technology
Temperature adaptive control
Phase change materials

ABSTRACT

Cooling demand in buildings accounts for a significant portion of global energy consumption and is estimated to increase tenfold by 2050. Daytime radiative cooling shows great potential for reducing surface temperatures and cooling energy consumption of buildings by dissipating heat into cosmic space without consuming any energy. However, further commercial application of radiative cooling technologies requires improvements in their cooling efficiency, reduction of manufacturing costs, and optimisation of their seasonal suitability. Meanwhile, typical daytime radiative coolers with constant solar spectral reflective and mid-infrared emissivity cannot automatically switch off in cold winter and would lead to an energy penalty for heating. To overcome the above limitations, this paper reviews the types of daytime radiative coolers in terms of their structure and related temperature-adaptive control methods. The literature is also analysed to compare and evaluate the performance indicators, design methods, numerical simulation methods and manufacturing processes of daytime radiative coolers. Furthermore, the insulation and convection shielding methods during daytime radiative cooling experiments are also critically reviewed. The study also summarises recently developed temperature-adaptive daytime radiative coolers that utilize a daytime radiative cooler with a switching accessory or temperature-switching material. This paper critically reviews the switching control technologies, switching accessories and materials for the temperature-adaptive daytime radiative cooler to analyze their characteristics and their effect on the heat transfer of daytime radiative coolers. Finally, the potential temperature-adaptive switching materials that can be used for temperature-adaptive daytime radiative coolers are presented. The review demonstrated that the higher the solar reflectance and mid-infrared emissivity of the daytime radiative cooler, the larger the cooling temperature drop during daylight. Mie theory, Maxwell's equations and finite difference time domain are commonly used for the design and simulation of daytime radiative coolers with commercial software. Daytime radiative cooler structures of nanoparticles in polymers, porous and random nanofibers structures are technically mature, less costly and suitable for mass production. The mechanical switching control system for daytime radiative cooling is sensitive, and the switching temperature can be set flexibly, but its limitations are complexity, durability and high cost. Temperature-adaptive switching materials (i.e. phase change materials and thermo-chromic materials) have the advantages of adaptive passive control and easy integration into daytime radiative coolers. Overall, this review contributes to guiding the development of radiative cooling technologies through the comparison of the cooling effect, manufacturing process, manufacturing cost, advantages and disadvantages of current control methods and materials for DRCers.

1. Introduction

Currently, heating and cooling in residential and commercial buildings consume approximately 40% of the world's energy supply,

with cooling representing a major part of the energy use in buildings, i.e. 50% in the US [1,2]. Meanwhile, it is estimated that the demand for cooling will increase tenfold by 2050 [3]. Radiative cooling technology [4] can achieve a cooling effect by radiating surface heat into the 3 K cosmic space [5], and has become a topical research area in the last few

* Corresponding author at: School of Mechanical Engineering, Qilu University of Technology (Shandong Academy of Sciences), 250353 Jinan, China.
E-mail address: wgsuper@hotmail.com (W. Su).

Nomenclature	
Abbreviations	
AAO	Anodic aluminium oxide
ALD	Atomic layer deposition
AZO	Al-doped ZnO
CNT	Carbon nanotube
DPHA	Dipentaerythritol penta-hexa-acrylate
DRC	Daytime radiative cooling
DRCer	Daytime radiative cooler
FDTD	Finite difference time domain
FSPCM	Form stable PCM
FTO	Fluorine doped tin oxide
HDPE	High-density polyethylene
HDTMS	Hexadecyltrimethoxysilane
IAD	Inverse adding-doubling method
IST	In ₃ SbTe ₂
ITO	Indium tin oxide
IR	Infrared
LDPE	Low-density polyethylene
MIR	Mid-infrared
NG	Not given
NIPAm	N-isopropylacrylamide monomer
NP	Nanoparticles
PCM	Phase change material
PDMS	Polydimethylsiloxane
PE	Polyethylene
PMMA	Polymethyl methacrylate
PSO	Particle swarm optimization
PTFE	Polytetrafluoroethylene
RCWA	Rigorous-coupled-wave analysis
SiOxNy	Silicon oxynitride
SMPs	Shape Memory Polymers
TADRCer	Temperature-adaptive radiative cooler
TCPCS	Temperature-controlled phase change structure
TMM	Transfer matrix method
TPX	Polymethylpentene
TSMPs	Temperature-adaptive shape memory polymer s switch
TSMS	Temperature shape memory spring
UV	Ultraviolet
VIS	Visible spectrum
Symbols	
h	Heat transfer (W/m ² °C)
P	Power density (W/m ²)
τ	Transmittance (%)
Subscripts	
c	Convective heat transfer coefficient
atm	The atmosphere absorbed thermal radiation
cond + conv	Conduction and convention heat transfer
net-cooling	Net cooling
rad	The emitted thermal radiation from the thermal emitter
solar	The absorbed thermal radiation from sunlight

years. In radiative cooling, heat will need to pass through the “8–13 μm atmospheric window” and the “16–25 μm atmospheric window” [6] to avoid the absorption of infrared waves. However, the “atmospheric window” for radiative cooling commonly refers to 8–13 μm, as 16–25 μm is strongly affected by atmospheric humidity [6]. Radiative cooling could therefore become a crucial and effective technique to reduce energy consumption for cooling and subsequently address issues on greenhouse gas emissions and global warming.

The daytime radiative cooling (DRC) technology has been designed and developed rapidly after the research of Rephaeli et al. [7] in 2012 and Raman et al. [8] in 2014. DRC technology utilizes radiative cooling principles to dissipate heat into space. The key innovation of DRC is that it achieves cooling even during the daytime when the sun’s radiation is intense. DRC has diverse applications in buildings, vehicles, and electronic devices, providing sustainable cooling without energy-intensive systems. It reduces energy demand, decreases carbon dioxide emissions, benefits regions with limited electricity access and improving thermal comfort in hot climates. The net cooling power ($P_{\text{net-cooling}}$) of daytime radiative cooler (DRCer) requires that the radiating flux of DRCer into cosmic space (P_{rad}) is larger than its total absorbing flux from the sunlight (P_{sun}), the incident atmospheric thermal radiation (P_{atm}) and the convection and conduction with the ambient environment ($P_{\text{cond+conv}}$) [5]. Therefore, the $P_{\text{net-cooling}}$ can be calculated by Eq.1 as follows [8]:

$$P_{\text{net-cooling}} = P_{\text{rad}} - P_{\text{sun}} - P_{\text{atm}} - P_{\text{cond+conv}} \quad (1)$$

At 300 K on earth, approximately 35% of the thermal radiation energy (cooling power of 160 W/m²) emitted by a blackbody is in 8–13 μm band wavelength range [9]. Meanwhile, 99% of the solar radiation energy received on earth is in the 0.2–3 μm band range [10] and DRCer must reflect at least 90% of the sunlight to achieve a net cooling [8]. According to equation (1), the DRC net-cooling power can be enlarged by the following four methods. (a) Using high solar spectral reflective materials to reduce P_{sun} , such as Ag, Al, etc. [5]. (b) Using high emissivity materials (i.e. Polydimethylsiloxane (PDMS) [11] and Si [12]) and

optimizing the optical structure [13,14] to increase the radiative cooling effect (P_{rad}) of a DRCer. (c) Setting DRCers at a location with typically low cloud cover can reduce P_{atm} . [6]. (d) Adding insulation and a cover shield to reduce cooling energy loss by convection and conduction ($P_{\text{cond+conv}}$) of DRCers [15]. Therefore, besides the DRC experimental atmospheric conditions, the materials, structures, and insulation methods of DRCers are key parameters for their cooling performance. To develop an efficient DRCer, this paper reviewed the different structures of various DRCers, such as multilayer structure [8], porous structure [16], the structure of nanoparticles in polymers [17], random nanofibers structure [18], photonic crystal structure [19], and hybrid structure [20–23]. Moreover, the cooling performance, design methods, numerical models, fabrication processes, insulation and convection shielding methods of these DRCers were critically reviewed and compared.

Typical static DRCers are unable to modulate their long-wave infrared wavelengths of thermal radiation in response to changes in cooling/heating demand [24]. In other words, static DRCers have constant optical properties (i.e. constant solar spectral reflection and mid-infrared emissivity). In hot summer, the application of radiative cooling could decrease cooling energy consumption. However, static radiative cooling may lead to overcooling and an increase in heating energy consumption in cold winter conditions [25]. To overcome this issue, researchers have proposed and developed temperature-adaptive daytime radiative coolers (TADRCers) [26], which could switch between two operating modes (switch-on and switch-off) in response to different ambient temperatures [27]. This paper summarizes current control methods for some typical TADRCers, such as mechanical switches for DRCer [26], integrated temperature adaptive switching materials for DRCers [28], and DRCers with temperature adaptive switching materials cover shields [27]. The comparison and analysis in this paper identify the limitations of the current TADRCers. Meanwhile, potential switching control materials for TADRCers are summarised to indicate the future research directions for TADRCers. Overall, this paper provides a research guideline for DRCers development, material selection, experimental methods, low-cost manufacturing and self-adaptive

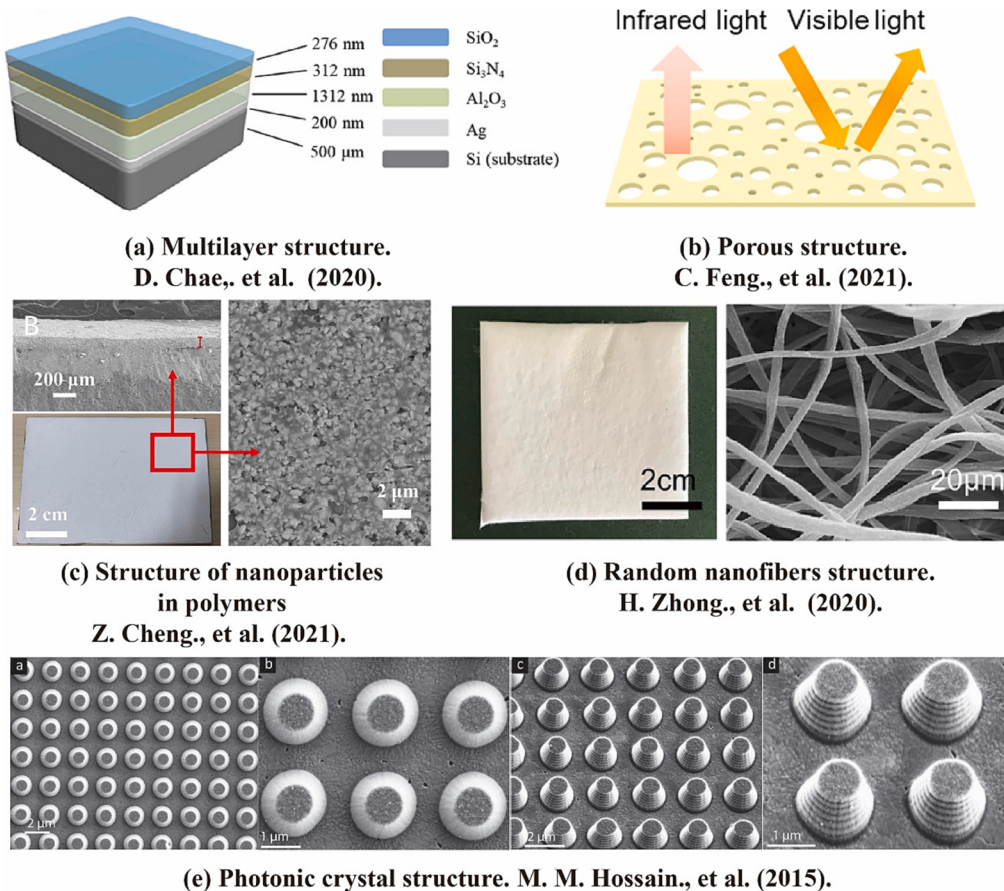


Fig. 1. The typical structures of DRCers (D. Chae., et al. 2020, copyright Adv. Opt. Mater; C. Feng., et al. 2021, copyright Nano Energy; Z. Cheng., et al. 2021, copyright Nano Energy; H. Zhong., et al. 2020, copyright ACS Nano; M. M. Hossain., et al. 2015, copyright Adv. Opt. Mater.) [19,29–32].

control methods based on a review of the current state-of-the-art in DRCers and the respective control technologies.

2. Daytime radiative cooler

2.1. Structures and materials

As shown in Fig. 1, the typical structures of a DRCer include multilayer structure, porous structure, the structure of nanoparticles in polymer, random nanofibers structure, and photonic crystal structure.

2.1.1. Multilayer structure

DRCers with multilayer structure have been extensively investigated which has two components: 1) the emissive layer (radiator) consisting of multiple layer materials, which could emit thermal radiation through the “atmospheric window” (8–13 μm); and 2) the reflective layer (reflector) with high reflectivity of the solar spectrum, which enables the DRCers to efficiently reflect the incident solar spectrum (0.2–3 μm), as shown in Fig. 1 (a). Common emissive layer materials include Si [12,29,33], Si_3N_4 [29,33–35], SiO_2 [8,29,34], SiCNO [36], HfO_2 [8], Al_2O_3 [29,35], ZnO , polytetrafluoroethylene (PTFE) [9], PDMS [11,12,37], etc. The reflectivity value of silver (Ag) and aluminium (Al) is as high as 0.97 and 0.94 [5] respectively, which makes Ag [8,11,12,29,34–36,38] and Al [9,33,36,37] the most common reflective materials for DRCers. For example, the DRCer fabricated by Raman et al. [8] could reflect 97% of the incident sunlight. This achieved a cooling power of 40.1 W/m^2 and dropped the DRC temperature by 4.9 $^\circ\text{C}$ when the sunlight intensity power was greater than 850 W/m^2 . Kou et al. [12] achieved DRC with 100 μm PDMS, 500 μm silica and 120 nm silver layers. The temperature drop of DRCer reached 8.2 $^\circ\text{C}$ and 8.4 $^\circ\text{C}$ for the

day and night, respectively. Chen et al. [33] designed a vacuum-encapsulated multilayer structure radiative cooling device with a maximum theoretical temperature reduction of 60 $^\circ\text{C}$, and demonstrated the peak temperature reduction to be as much as 42 $^\circ\text{C}$ with a 24-hour experiment.

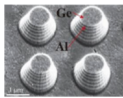
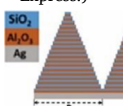
Overall, the multilayer structures of DRCers are usually composed of emissive layers (i.e. Si, Si_3N_4 , SiO_2 , and PDMS) and a silver or aluminium reflective layer. However, the materials and production costs for multilayer structures DRCers are relatively expensive. Future research directions should involve optimizing multilayer structures, ensuring durability and stability, scalability for mass production, integration with existing systems, and addressing energy efficiency and economic viability.

2.1.2. Porous structure

Porous polymer materials with light-scattering air voids can effectively scatter light and increase thermal emissivity. Therefore, the porous structure can achieve efficient daylight reflection [16]. As shown in Fig. 1 (b), Feng et al. [30] used Li-PAAm hydrogel, poly (vinylidene fluoride-co-hexafluoropropene) [P(VdF-HFP)] and the phase inversion method to prepare a bilayer porous polymer film DRCer with three pore diameter peaks at 0.4 μm , 3 μm and 100 μm . With the synergistic effect of hydrogel evaporative cooling, the bilayer of hygroscopic hydrogel and hydrophobic porous polymer film attained a remarkable temperature drop of 7 $^\circ\text{C}$ and cooling power of 150 W/m^2 under direct sunlight. Wang et al. [39] fabricated a DRCer with PMMA porous structure which has 5 μm pores, 0.95 solar reflectivity and 0.98 emissivity. The daytime cooling temperature dropped by 6 $^\circ\text{C}$ at a solar radiation power of 900 W/m^2 , relative humidity of 40%, and the night cooling temperature dropped by 8.2 $^\circ\text{C}$. Weng et al. [40] prepared a porous

Table 1

Summary of photonic crystal structures (S = Simulation, E = Experiment).

Structure & materials illustration	Reflectance (Negative sign represents absorption)	Emissivity	Cooling temperature (°C)	Net cooling power (W/m ²)	Reference
	0.97(S)	0.99(S), 0.90 (E)	12.2 (E, daytime)	116.6 (E)	Hossain et al. 2015 [19]
(M. M. Hossain., et al. 2015, copyright Adv. Opt. Mater.)					
	-0.95(E)	0.99(E)	reduced 13 °C of absorber temperature	-	Zhu et al. 2015 [57]
(L. Zhu., et al. 2015, copyright Proc Natl Acad Sci U S A)					
	0.90(S)	0.98(S)	11.4(S, daytime) 8.2(S, night)	-	Zou et al. 2017 [55]
(C. Zou., et al. 2017, copyright Adv. Opt. Mater.)					
	-	0.85(S)	-	-	Liu et al. 2017 [56]
(T. Liu., et al. 2017, copyright Opt Express.)					
	0.99(S)	0.99(S)	-	122 (S)	Wu et al. 2018 [54]
(S. R. Wu., et al. 2018, copyright Sci Rep.)					

polydimethylsiloxane sponge emitter with NaCl template with an average size of 6 μm and the mass ratio of NaCl against PDMS in the range of 0.5% to 5%. The DRCer achieved 0.95 solar spectrum reflectance and average emissivity of 0.97, which resulted in 8 °C temperature drop in ambient conditions under a daylight radiant power of 837 W/m².

The advantages of porous structures DRCers include: 1) they can effectively scatter light between the interface of polymer and air; 2) they can be fabricated by solution-based and scalable methods, such as freeze-drying, phase separation, or electrospinning [41,42] and; 3) their ability to be integrated with other functional materials (i.e. phase change materials) to improve cooling performance. However, porous structures DRCers are also limited by low mechanical strength and their low thermal conductivity, while being prone to water condensation and dust accumulation. Therefore, future research should focus on developing new materials with high solar reflectance and thermal emittance in a wide wavelength range, optimizing the structure design and fabrication parameters to achieve high porosity and uniform pore distribution, and exploring new applications in building cooling and energy-saving fields.

2.1.3. Structure of nanoparticles in polymers

Randomly doping some specific nanoparticles into polymer materials can fabricate a radiative cooler, see Fig. 1 (c) [43]. This is because the doped nanoparticles would result in Mie scattering of sunlight and achieve high emissivity in the “atmospheric window” by resonance effect [43].

DRCers with the structure of nanoparticles in polymers are mainly inorganic materials, such as SiO₂ (90 nm [44], 400 nm [31]), TiO₂ (200–250 nm [44]), CaCO₃ (500 nm [17]), BaSO₄ (400 nm [31]), Al₂O₃ [45,46], SiC (50 nm [47,48]), ZrO₂ (500 nm [43]), etc. Li et al. [17] demonstrated a single-layer particle–matrix CaCO₃-acrylic paint for radiative cooling. The paint reflected 96% of solar radiation and emitted 94% mid-infrared (MIR) in atmospheric window that showed cooling power over 37 W/m² and dropped the surface temperature by 1.7°C at noon. The structure of the DRCer was improved by fabricating

150 μm BaSO₄ particle film on a silicon wafer. The average diameter of BaSO₄ pellets was 400 nm, and the mass mixing ratio of BaSO₄: deionized water: ethanol was 2:1:1 [49]. After painting and drying, its sunlight spectral reflectance and emissivity were as high as 0.98 and 0.96, respectively. The daytime cooling effect was 10.5 °C below the ambient temperature when sunlight intensity and ambient relative humidity were at 907 W/m² and 64%, respectively. The cooling temperature was 8.8 °C lower than the previous CaCO₃-acrylic paint.

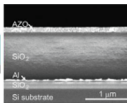
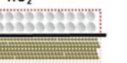
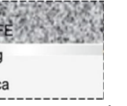
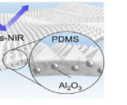
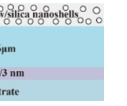
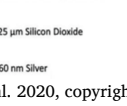
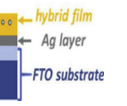
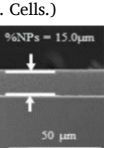
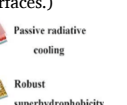
Generally, nanoparticle structures DRCers can achieve higher cooling power than bulk materials by enhancing radiative cooling in the atmospheric window. Nanoparticle structures DRCers can be easily fabricated by spin coating, dip coating or spray coating [50] and are scalable for different applications. However, nanoparticle structures DRCers have higher fabrication costs, use often toxic or rare materials during fabrication and have lower durability than structures of bulk materials. They also have limited performance under certain conditions, such as overcast or humid weather, when accumulating dust and when the ambient temperature is high [51]. To this end, this review recommends the development of designs of new nanoparticle structures DRCers that can achieve higher cooling power, are of lower cost, have higher durability and have a lower environmental impact. Furthermore, the long-term performance and life cycle assessment of nanoparticle structures DRCers under different scenarios and locations should be studied. Meanwhile, new applications of nanoparticle structures DRCers for thermophotovoltaics, rectennas, infrared detectors, and emissive energy harvesters should also be part of future research investigations.

2.1.4. Random nanofibers structure

The emission in the MIR region is typically associated with molecular bonding, which enables narrow band and selective absorption/emission in the MIR region [18]. Therefore, utilizing some materials with specific chemical bonding can provide a particularly convenient and scalable pathway to achieve DRC. Meanwhile, fabricating this type of DRCers is much more simple and easier compared to complex top-down fabrication methods, as shown in Fig. 1(d) [32]. For the production of DRCers with random nanofibers structure, the vibrational absorptions should be

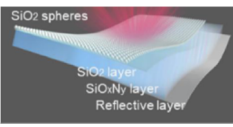
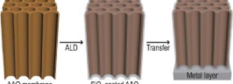
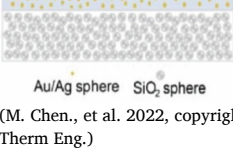
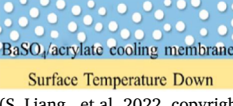
Table 2

DRCers with hybrid structure (D-daytime, N-nighttime).

Hybrid structures	Structure & materials illustration	Preparation methods	Cooling temperature (°C)	Reflectivity (0.2–3 μm)	Emissivity (8–13 μm)	Reference & Author
Multilayer & photonic crystal	 (K. Sun., et al. 2017, copyright ACS Photonics.)	Coating, depositing, ion beam etch process	–	0.84	0.79	Sun et al. 2017 [23]
Multilayer & nanoparticles	Copyright permission not obtained	Roll-to-roll manner, electron beam evaporation	8 (D)	0.96	0.93	Zhai et al. 2017 [22]
Multilayer & nanoparticles	 (H. Bao., et al. 2017, copyright Sol. Energy Mater. Sol. Cells.)	Spraying coating method	TiO ₂ + SiC: 8 (D), 4 (N) TiO ₂ + SiO ₂ : 6 (D), 5(N)	0.90	0.90	Bao et al. 2017 [65]
Multilayer & porous	 (H. Zhong., et al. 2020, copyright ACS Appl. Mater. Interfaces.)	Facile coating-and-pressing method, electron beam evaporation	2.7 (D) 7 (N)	0.98	0.90	Zhong et al. 2020 [20]
Multilayer & nanoparticles & photonic crystal	 (H. Zhang., et al. 2020, copyright Proc Natl Acad Sci U S A.)	Photolithography, dry etching, wet etching, spin coating, and stripping	5.1 (D)	0.95	0.96	Zhang et al. 2020 [21]
Multilayer & nanoparticles		Resistive heating evaporation, spin-coating,	2.3 (D)	0.98	0.90	Suichi et al. 2020 [61]
Multilayer & photonic crystal	 (S. Y. Jeong., et al. 2020, copyright Sol. Energy Mater. Sol. Cells.)	Photolithography, advanced oxide etching, spinning coating, curing	6.2 (D)	0.97	0.98	Jeong et al. 2020 [62]
Multilayer & nanoparticles	 (J. Yang., et al. 2020, copyright Sol. Energy Mater. Sol. Cells.)	Tape casting method	20 (lower than the black surface, D) 4.5 (N)	0.96	0.91	Yang et al. 2020 [66]
Multilayer & nanoparticles	 (Y. Liu., et al. 2020, copyright Sol. Energy Mater. Sol. Cells.)	Spraying coating and spinning coating	10 (D) 2.5 (N)	0.95	0.91	Liu et al. 2020 [67]
Multilayer & nanoparticles	 (D. Chae., et al. 2021, copyright ACS Appl. Mater. Interfaces.)	One-step spin coating without many vacuum deposition processes	3.4 (D) 6.3 (N)	0.96	0.88	Chae et al. 2021 [35]
Multilayer & porous	 (S. Wang., et al. 2021, copyright ACS Appl. Mater. Interfaces.)	Facile one-step plasma-induced thermal-field assisted oxidation and cross-linking (PTOC) method	3.6 (D)	0.88	0.92	Wang et al. 2021 [63]

(continued on next page)

Table 2 (continued)

Hybrid structures	Structure & materials illustration	Preparation methods	Cooling temperature (°C)	Reflectivity (0.2–3 μm)	Emissivity (8–13 μm)	Reference & Author
Multilayer & nanoparticles	 (C. Lin., et al. 2021, copyright Researchsquare)	Facile solution processes	5 (D)	0.96	0.94	Lin et al. 2021 [68]
Multilayer & porous	 (D. Lee., et al. 2021, copyright Nano Energy.)	Two-step anodization	6.1 (D)	0.86	0.96	Lee et al. 2021 [69]
Multilayer & nanoparticles	 (D. Chae., et al. 2021, copyright Mater. Today Phys.)	Spray-coating, drop-casting	8.8 (N)	0.96	0.93	Chae et al. 2021 [70]
Multilayer & nanoparticles	 (M. Chen., et al. 2022, copyright Appl Therm Eng.)	General chemical preparation method.	10.9 (D)	0.94	0.93	Chen et al. 2022 [64]
Multilayer & nanoparticles	 (S. Liang., et al. 2022, copyright ACS Omega.)	General chemical preparation method.	4.4 (D)	0.99 (in UV band)	–	Liang et al. 2022 [71]

in the wavelength of 8–13 μm and the wave number range in 769–1250 cm⁻¹. To this end, the bonds C–O–C (1,260– 1,110 cm⁻¹), C–OH (1,239–1,030 cm⁻¹), –CF₃ (1,148 cm⁻¹) and Si–O–Si (1,100 cm⁻¹) in polymers have great potential as a thermal emitter [18].

Li et al. [52] used polyethylene oxide to fabricate nanofiber structures through the roll-to-roll electrospinning fabrication method. These structures had a reflectivity of 0.96 solar radiation and 0.78 emissivity in the “atmospheric window”. The temperature dropped 5 °C and achieved a net cooling power of 110 W/m² during an outdoor test (wind speed 1–11 m/s, relative humidity 30% to 97%, and solar radiation flux 900 W/m²). Zhong et al. [53] used AlPO₄, cotton fabric and PDMS as raw materials to produce a nanofibrous DRCer by the precipitation method. 90% of the sunlight was reflected, while the emissivity under the “atmospheric window” reached 0.92. The average temperature of the DRCer was 5.4 °C lower than the reference sample under direct sunlight at 37 °C and 998 W/m² of solar radiation. Zhong et al. [32] used polyvinylidene fluoride and poly(vinyl alcohol) as raw materials to produce a nanofiber structure through the electrospinning process. The nanofiber structure showed 0.94 reflectance of the solar spectrum and 0.94 emissivity in MIR. The DRCer achieved a temperature drop of 9 °C when solar radiation power was 900 W/m² during an outdoor test.

In summary, further research should focus on exploring alternative materials or combinations of materials that possess the desired chemical bonding properties for achieving high emissivity in the MIR region. This could involve investigating novel polymers or composite materials that exhibit strong vibrational absorptions within the specified wavelength and wave number ranges. Additionally, the focus of future work should explore different fabrication methods or techniques to enhance the scalability of producing random nanofiber structures DRCers.

2.1.5. Photonic crystal structure

Photolithography can manufacture high-precision three-dimensional

structures on the surface of the material, which can control its emissivity and reflectivity properties to achieve the DRC. However, the majority of the research studies hitherto report theoretical designs and simulations due to the high manufacturing cost and threshold of photolithography [7,19,54–56], albeit a small number of experimental studies have also been reported [19,57], see Table 1.

Rephaeli et al. [7] studied theoretically a photonic crystal structure with stacking radiative emission layers below a broadband chirped reflector. The optimized DRCers consist of two thermally emitting photonic crystal layers comprised of SiC and quartz. In this case, the reflector consists of three sets of five bilayers made of MgF₂ and TiO₂ with varying periods on a silver substrate. The theoretical cooling power of this DRCer was up to 100 W/m². Wu et al. [54] also numerically studied a near-ideal radiative cooler with a theoretical net cooling power more than 122 W/m², which could achieve selective MIR emissivity and low absorption in the solar spectrum.

Hossain et al. [19] used silicon, aluminum and PMMA as raw materials to produce conical metamaterial by the electron-beam evaporation and Electron-beam lithography methods. The emitter test cooling power reached 116.6 W/m² and cooled down by 12.2 °C. Zhu et al. [57] used electron beam evaporation and photolithography methods to fabricate a visibly transparent thermal blackbody from a p-doped double-side-polished crystalline silicon wafer. When the silicon absorber was placed under sunlight, the blackbody without a reflective layer reduced the temperature of the underlying silicon absorber by 13 °C.

In summary, the development of cost-effective manufacturing techniques for photolithography should be the focus of future work. For instance, enabling wider practical implementation of high-precision three-dimensional structures with controlled emissivity and reflectivity properties, exploring alternative materials, process optimizations, and innovative fabrication methods to reduce the manufacturing cost and threshold associated with photolithography.

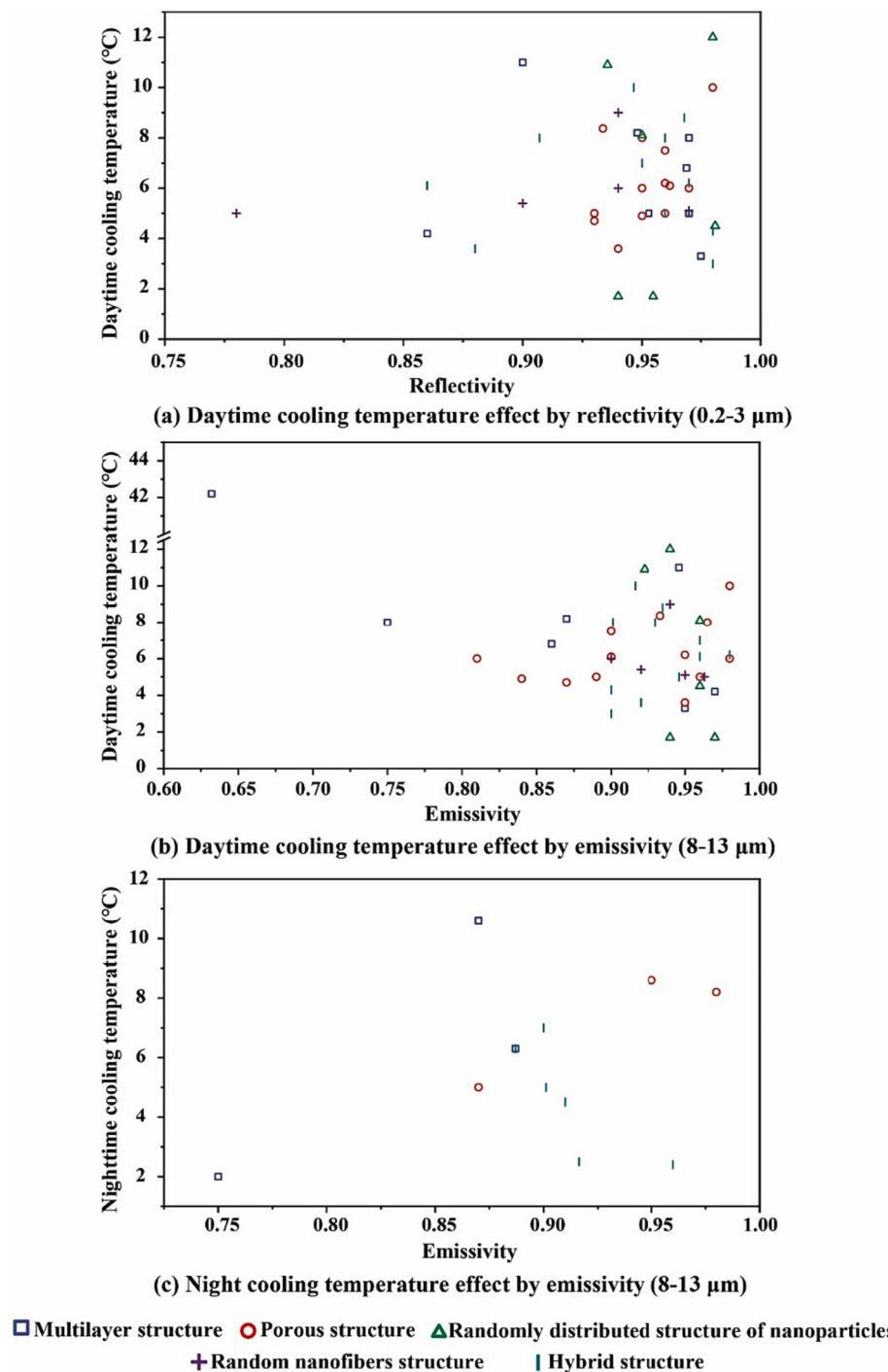


Fig. 2. Cooling capacity of various DRCers. Note: Multilayer structure [8,9,11,12,29,33–38], Porous structure [16,30,39,40,73–83], Randomly distributed structure of nanoparticles [17,31,43,44,49,72,84], Random nanofibers structure [18,32,53,85,86], Hybrid structure [6,7,20–23,35,58,59,61–63,65–70,87].

2.1.6. Hybrid structure

Most of the DRCers with hybrid structures are based on a combination of multilayer structures with the other structures, such as multilayer structure & nanoparticles structure, multilayer structure & porous structure, multilayer structure & photonic crystal structure and multilayer structure & nanoparticles structure & photonic crystal structure. Most of the hybrid structures are contained within a high reflectivity bottom material layer, such as Al [48,58] and Ag [22,59–61], see Table 2.

In 2017, Sun et al. [23] fabricated a DRCer with a multilayer & photonic crystal structure by chemical vapour deposition and the e-

beam lithography method. This method used an Al-doped ZnO transparent conducting oxide as infrared plasmonic material to produce a metasurface. The solar reflectance and thermal emissivity for the optimized hybrid structure were 0.84 and 0.79, respectively. Zhai et al. [22] manufactured a DRCer with a multilayer & nanoparticles structure by embedding resonant polar dielectric microspheres randomly in a polymeric matrix with back silver coating. This resulted in a metamaterial with an infrared emissivity of over 0.93 and radiative cooling power of 93 W/m^2 at noon. Moreover, the manufacturing cost of this material was much lower than that of Sun et al. who used lithography [23].

As shown in Table 2, the other hybrid structures have been

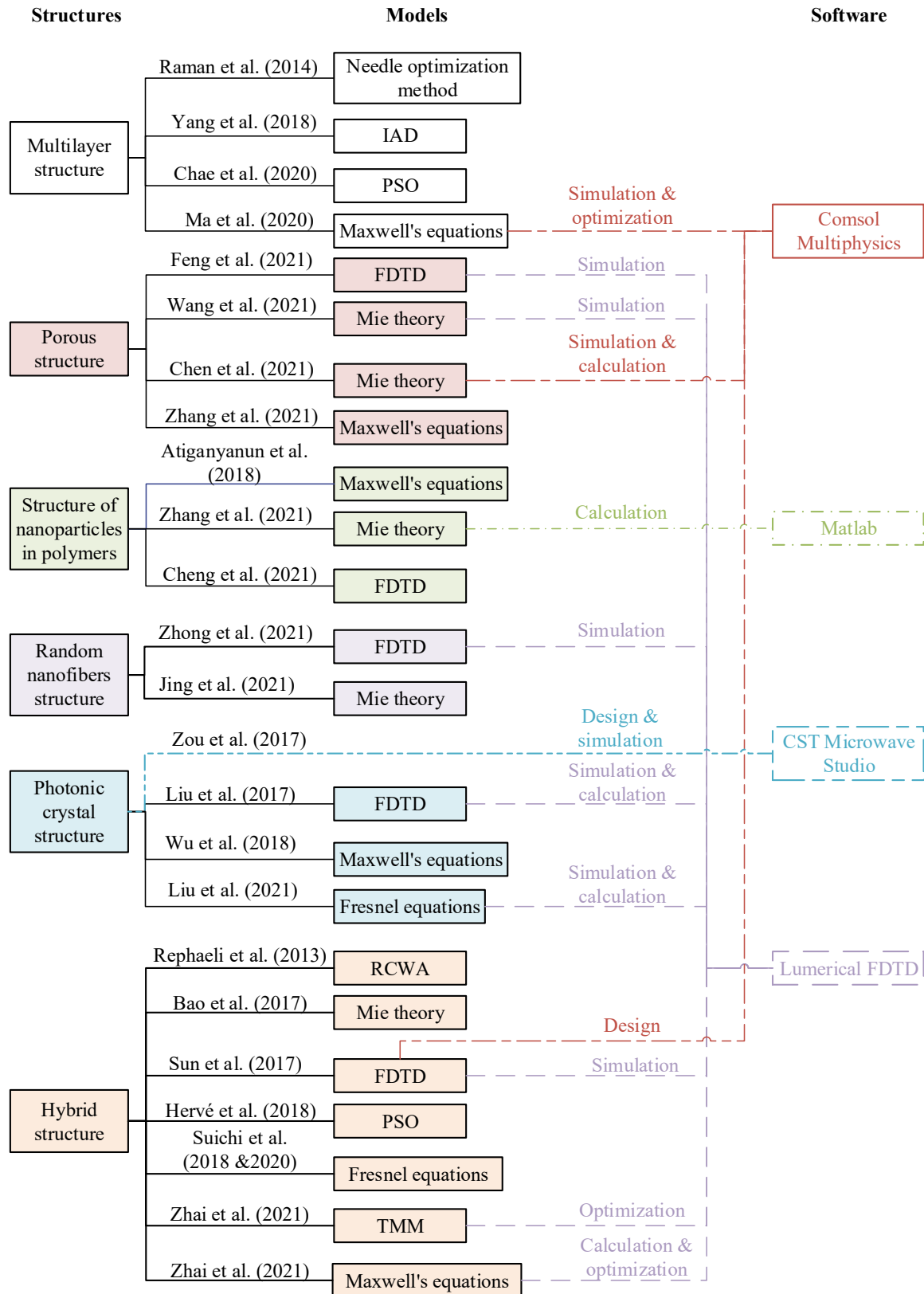


Fig. 3. Structures and software corresponding to simulation and calculation. note: multilayer structure raman et al. [8], Chae et al. [29], Yang et al. [9], Ma et al. [34]. Porous structure: Feng et al. [30] Wang et al. [39], Chen et al. [82], Zhang et al. [75]. Structure of nanoparticles in polymers: Cheng et al. [31], Zhang et al. [43], Atiganyanun et al. [44]. Random nanofibers structure: Zhong et al. [32], Jing et al. [85]. Photonic crystal structure: Liu et al. [56], Wu et al. [54], Liu et al. [56], Zou et al. [55]. Hybrid structure: Sun et al. [23], Rephaeli et al. [7], Hervé et al. [87], Bao et al. [65], Zhai et al. [58], Suichi et al. [6,61].

developed to improve upon the performance of DRCers. Especially, the DRCers with multilayer & nanoparticles & photonic crystal structures produced by Jeong et al. [62] achieved a maximum emissivity of 0.98, which is higher than that of other multilayer structures. In 2020, Zhang et al. [21] and Jeong et al. [62] fabricated hybrid DRCers through photolithography and spinning coating, which resulted in DRCers with reflectances of 0.95 and 0.97 in the solar spectrum and IR emissivities of 0.96 and 0.98, respectively. However, those methods were found to be complex and expensive. Therefore, Wang et al. [63] and Chen et al. [64] fabricated hybrid DRCers with some low-cost preparation methods (i.e. general chemical reactions) to achieve radiative cooling through experiments in 2021 and 2022. However, the solar reflectance (0.88 and 0.94) and IR emissivity (0.92 and 0.93) of those two kinds of DRCers were lower than what was obtained by Zhang et al. [21] and Jeong et al. [62] in 2020.

Further research in the field of DRCers could focus on developing hybrid structures that combine multilayer structures with additional elements to enhance their performance. These elements could include nanoparticles, porous structures, and photonic crystal structures. Previous studies have demonstrated the potential of such hybrid structures, but there is space for improvement in terms of cost-effectiveness and simplicity of fabrication methods. Researchers could explore alternative low-cost preparation methods, such as general chemical reactions, while aiming to maintain high performance in terms of solar reflectance and IR emissivity.

2.1.7. Performance evaluation of DRCers types

The cooling capacity of different types of DRCers is compared in Fig. 2. In general, the higher the solar reflectance and infrared emissivity, the larger the cooling temperature drop during daytime; the higher the emissivity, the larger the cooling capacity at night. However, some DRCers with a reflectivity of 0.90–0.98 demonstrated significant differences in cooling temperature performance in Fig. 2 (a). For example, for the same structure of nanoparticles in polymers with 0.94 reflectivity, Zhang et al. [43] showed a cooling of 10.9 °C under daylight, but the cooling temperature in the experiment of Huang et al. [72] was only 1.7 °C under daylight. The different results may be caused by the following three reasons: (a) The emissivity of the DRCer of Zhang et al. was 0.92 [43], while the value of Huang et al. was 0.97 [72]. That means the P_{rad} in Zhang et al. was larger which leads to a higher $P_{net-cooling}$; (b) During the outdoor experiments, the solar spectral radiant power was 895 W/m² for Zhang et al. [43] and 1100 W/m² for Huang et al. [72], which resulted in different P_{sun} ; (c) The insulation method/materials used by Zhang et al. [43] is more effective than Huang et al. [72] and resulted in lower $P_{cond+conv}$. Zhang et al. [43] insulated the DRCer by extruding polystyrene board wrapped with aluminium foil and low-density polyethylene (LDPE) cover. However, Huang et al. [72] used a transparent polycarbonate box cushioned with polystyrene foam without a cover shield during the experiment.

The above comparison shows the performance of DRCers is affected by the experimental boundary conditions, the reflectivity and emissivity and the thermal insulation method of the experimental rig. DRCers show a better daytime cooling performance when the experiments are undertaken during low solar radiation and high atmospheric transmittance days. This is because the DRCers could significantly increase the sunlight reflectance and the infrared emissivity in the “atmospheric window”. Chen et al. [33] realized a day temperature drop of 42.2 °C by a DRCer which had a multilayer stack of Si₃N₄, Si and Al structure, and measured cooling temperature far higher than that of the other multilayer structures, as shown in Fig. 2. This is due to the DRCer being isolated by a ZnSe radiation window in a vacuum chamber, which means P_{sun} and $P_{cond+conv}$ were close to zero during the experiment.

The performance of DRCers is affected by the experimental environmental conditions, the reflectivity and emissivity of DRCer, and the thermal insulation method and materials of the experimental rig. The review demonstrated that the higher the solar reflectance and MIR

Table 3
Comparison of experimental and simulation results

Software	Simulation Ambient temperature setting (°C)	Solar radiation power (W/m ²)	hc (W/m ² K)	Net cooling power(W/m ²)	Cooling (°C)	Experiment Ambient temperature (°C)	Solar radiation power(W/m ²)	hc (W/m ² K)	Net cooling power(W/m ²)	Cooling (°C)	Reference
Comsol Multiphysics	–	AM1.5	6.9	40	–	–	800–870	–	–	40.1	4 ~ 5
	27	AM1.5	6.9	40 ~ 130	–	–	900	–	59.7 ~ 152.8	–	Raman et al. 2014 [8]
	20	AM1.5	12.5	72.7	4.3	14 ~ 26	760	–	–	–	Yang et al. 2020 [38]
Matlab	30	AM1.5	6.9	–	10	–	–	–	–	–	Zhu et al. 2021 [11]
	27	0	0	72.6	8.3	–0.1	0	6	–	6	Tao et al. 2021 [59]
										6.3	Chae et al. 2021 [35]

Table 4

Common fabrication processes of DRCers.

Structure	Craftsmanship	Complexity of process	Costs	Mass production evaluation	Related references
Multilayer structure	Dip-coating	Simple	Low	Suitable	[36]
	Solution-coating	Simple	Low	Suitable	[37]
	Spin-coating	General	Low	Suitable	[11,12]
	Evaporation	Sophisticated	High	Unsuitable	[8,11,29,33,34,38]
Photonic crystal structure	Photolithography	Sophisticated	High	Unsuitable	[55–57]
	Lithography	Sophisticated	High	Unsuitable	[19,55]
	Deposition	Sophisticated	High	Unsuitable	[19,54]
	E-beam patterning	Sophisticated	High	Unsuitable	[54]
	Etching	Sophisticated	High	Unsuitable	[54]
Randomly distributed structure of nanoparticles	colloidal sedimentation	Simple	Low	Suitable	[44]
	Roller coating	Simple	Low	Suitable	[31]
	1) Mixing and curing. 2) Coating. 3) Drying.	Simple	Low	Suitable	[31,49,84]
	Doctor-blade painting	Simple	Low	Suitable	[43]
Porous structure	Ball milling	Sophisticated	High	Unsuitable	[31]
	Air-spraying ethanolic & heat press	Simple	Low	Suitable	[78]
	Phase-inversion-based method	Simple	Low	Suitable	[16,77,82]
	Drop casting, bar coating, and scrape coating	Simple	Low	Suitable	[83]
Random nanofibers structure	Facile one-step thermal treatment	Simple	Low	Suitable	[82]
	Locally confined polymerization method	Simple	Low	Suitable	[81]
	Two-step anodisation process	Simple	Low	Suitable	[80]
	Two-step (hydraulic press and thermal annealing) and bottom-top (microparticles to bulk) synthetic procedure	Simple	Low	Suitable	[79]
	1) Mixing. 2) Curing.	Simple	Low	Suitable	[40]
	Phase separation-based method	Simple	Low	Suitable	[76]
	1) Melt-mix. 2) Compress. 3) Ultrasonic. 4) Extraction.	Simple	Low	Suitable	[74]
	1) Molding. 2) extrusion. 3) 3D printing.	Simple	Low	Suitable	[73]
	Medium embedding-extracting method	Sophisticated	High	Unsuitable	[39]
	Hot-pressing process	Simple	Low	Suitable	[86]
Hybrid structure	Electrospinning	Simple	Low	Suitable	[18,32]
	Facile electrospinning method	Simple	Low	Suitable	[85]
	Dipping, spraying, curing	Simple	Low	Suitable	[53]
	Spraying coating method	Simple	Low	Suitable	[65]
	Facile solution processes	Simple	Low	Suitable	[68]
	1) Spraying coating. 2) Spinning coating.	Simple	Low	Suitable	[67]
	1) Spray-coating. 2) drop-casting.	Simple	Low	Suitable	[70]
	1) Mixing. 2) Spin-coating, 3) Curing	Simple	Low	Suitable	[58]
	Two-step anodization	Simple	Low	Suitable	[69]
	A facile one-step plasma-induced thermal-field assisted oxidation and cross-linking (PTOC) method	Simple	Low	Suitable	[63]
	Photolithography	Sophisticated	High	Unsuitable	[7]
	1) Coating. 2) depositing. 3) ion beam etch process	Sophisticated	High	Unsuitable	[23]
	1) Depositing. 2) photolithography.	Sophisticated	High	Unsuitable	[87]
	1) Photolithography. 2) Advanced oxide etching (AOE). 3) Spinning coating. 4) Curing.	Sophisticated	High	Unsuitable	[62]
	1) Photolithography. 2) Dry etching. 3) Wet etching. 4) Spin coating. 5) Stripping	Sophisticated	High	Unsuitable	[21]
	1) Dissolve. 2) Ball-milled. 3) Dispersed.	Sophisticated	High	Unsuitable	[59]
	1) Resistive heating. 2) uniformly Spin-coating.	Sophisticated	High	Unsuitable	[61]
	The tape casting method.	Sophisticated	High	Unsuitable	[66]
	One-step spin coating	Sophisticated	High	Unsuitable	[35]
	1) Produced in a roll-to-roll manner. 2) Electron beam evaporation	Sophisticated	High	Unsuitable	[22]
	1) Facile coating-and-pressing method. 2) Electron beam evaporation	Sophisticated	High	Unsuitable	[20]

emissivity of DRC, the larger the cooling temperature drops during daylight; and the higher the emissivity, the larger the cooling capacity at night. Generally, DRCers show a better daytime cooling performance when the experiments are undertaken during low solar radiation and a high atmospheric transmittance day.

2.2. Design and simulation methods

The optical properties and performance of DRCers are influenced by their constituent material and their macro and micro structures. The design and optimization methods for DRCers are also key factors for their development. To this end, the structures, mathematic models and software corresponding to simulation and calculation are summarized and shown in Fig. 3. The design methods of multilayer and hybrid

structure include finite-difference-time domain (FDTD) [11,20,21,23,34,58,62,65,68,69], rigorous-coupled-wave analysis (RCWA) [7,22,69,87], transfer matrix method (TMM) [58], needle optimization method [8], particle swarm optimization (PSO) [29,87], the inverse adding-doubling method (IAD) [9], Mie theory [35,65], Maxwell's equations [11,34] and Fresnel equations [6,61,70]. Simulation and design methods for photonic crystal structure include finite-difference-time domain (FDTD) [54,56], Maxwell's equations [54]. Simulation and design methods for porous structures include finite-difference-time domain (FDTD) [16,30,39,40,74–76,78–80,82], Mie theory [39,74,75,82], and Maxwell's equations [74,75,80]. Simulation and design of randomly doped structures of polymer nanoparticles by the finite-difference-time domain (FDTD) [31,44], Mie theory [17,31,43,49,84], Maxwell's equations [44]. For nanofibre-polymer

Table 5

Insulation in DRC experiments (D-daytime, N-nighttime).

Reference & Author	Thermal insulation material	Transmittance (0.2–2.5 μm)	Emissivity (8–13 μm)	h_e (W/ m^2K)	Net cooling power (W/ m^2)	Cooling temperature (°C)
Raman et al. 2014 [8]	Wood frame, Aluminium mylar, PMMA,Polystyrene	0.97	—	6.9	40.1 ± 4.1	5 (D)
Chen et al. 2016 [33]	Vacuum chamber	Shielded	0.63	0 ~ 8	90 ~ 105	42.2 (D)
Bao et al. 2017 [65]	Polystyrene, aluminium film	0.907	0.90	10	—	5 (N)
Kou et al. 2017 [12]	Aerogel blanket,Petri dish,	—	—	10	127	8.2 (D) 8.4 (N)
Suichi et al. 2018 [6]	PMMA chamber, Aluminized wood frame	0.89	0.89	12	—	2.8 °C above ambient (D)
Zhou et al. 2019 [37]	Foam container,aluminium foils	0.9	0.95	— —	90 ~ 120 76.3	11 (D) 6 (D) 9 (N)
Chae et al. 2020 [29]	Wooden frame, PMMA plate	0.95	0.87	6	66.4	8.2 (D) 10.6 (N)
Ma et al. 2020 [34]	PMMA Petri dish	0.97	0.75	6.9	56 ~ 87	8 (D) 2 (N)
Yang et al. 2020 [38]	PMMA dishes,Board box was wrapped in aluminium foils	0.95	—	6.9	60	5 (D)
Zhong et al. 2020 [20]	A box made of polystyrene; covered with aluminium mylar	0.98	0.9	8	120.6 (D) 140.1 (N)	3 (D) 7 (N)
Banik et al. 2021 [36]	Petri dish	0.97	0.86	10	93.7	6.8 (D)
Tian et al. 2021 [78]	Cooler box covered aluminium insulation	0.93	0.89	—	82.3(D) 71.6 (N)	5 (D)
Zhai et al. 2017 [22]	Foam container	0.96	0.93	5	72 h Average:110 93(D)	8 (D)
Atiganyanun et al. 2018 [44]	Styrofoam covered with aluminium sheets	0.98	0.94	—	—	12 (D) 4 (N)
Li et al. 2020 [17]	Styrofoam,Silver mylar	0.96	0.94	5	140	1.7 (D) 10 (N)
				—	56(N) 37(D)	—
Liu et al. 2020 [67]	Polystyrene surface is covered with aluminium foil	0.95	0.92	6	106	10 (D) 2.5 (N)
Chae et al. 2021 [35]	The wooden frames were covered with aluminium foil. PMMA,Polystyrene	0.96	0.89	6	72.6	6.3 (N)
				—	—	2.8 (D)
				—	—	2.7 (N)
				—	—	1 (D)
Chae et al. 2021 [70]	Aluminium tape,Polystyrene	0.97	0.94	12	—	8.8 (D)
				12	100.3	6.2 (D)
				—	—	10.9 (D)
				—	—	8.2 (D)
Chowdhury et al. 2021 [84]	Box covered with aluminium foil.	—	—	8.9	78	3.7 (D)
Li et al. 2021 [49]	Styrofoam enclosed by a silver mylar	0.98/0.98	0.96/0.95	— — —	117 110 80	10.5 (D) — —
Son et al. 2021 [90]	PMMA Wood frame Aluminium foilpolystyrene	white: 0.86 green:0.81red:0.78	0.97	6	—	White: 4.2 (D) Green: 3.6 (D) Red: 1.7 (D) White: 6.3 (N) Green:6.7 (N) Red:6.7 (N)
Tao et al. 2021 [59]	Polystyrene	—	—	6.9	—	6 (D)
Zhang et al. 2021 [43]	Polystyrene wrapped with a layer of aluminium foil	0.94	0.92	0/4/6/ 8	-/109/135/161	10.9 (D) 7.4 (N)
Son et al. 2020 [83]	Wooden frame PMMA Wooden frame was covered with an aluminium tapePolystyrene foam sheet covered with an aluminium foil	0.93	0.93	— —	—	8.37 (D) 11.3 (D)
Chen et al. 2021 [82]	A foam boxes wrapped in aluminium foil.	0.98	0.98	—	—	10 (D)
Feng et al. 2021 [30]	Acrylic sheets covered with aluminium foil as frame and polystyrene foam	0.96	0.96	—	114	5 (D)
Gao et al. 2021 [81]	Foam box with aluminium foil Copper platePolyethylene	0.96	0.90	0/3/8	100	7.5 (D)
Huang et al. 2021 [72]	Polycarbonate boxPolystyrene foam.	0.94	0.97	12	— —	1.7 (D) 9.5 (D)

(continued on next page)

Table 5 (continued)

Reference & Author	Thermal insulation material	Transmittance (0.2–2.5 μm)	Emissivity (8–13 μm)	h_c (W/m ² K)	Net cooling power (W/m ²)	Cooling temperature (°C)
Lee et al. 2021 [69]	Wooden frame PMMA	0.86	0.96	4/6/8	65.6	6.1 (D) 2.4 (N) —
Tian et al. 2021 [79]	Aluminium tape Polystyrene	—	—	—	—	—
Wang et al. 2021 [63]	Polyvinyl chloride insulation foam	0.94	0.95	—	124	3.6 (D)
Wang et al. 2021 [39]	Polystyrene frame covered by aluminium foil Polyethylene	0.88	0.92	—	—	3.6 (D)
Weng et al. 2021 [40]	Foam covered by a layer of reflective foil.	0.95	0.98	—	—	6 (D) 8.2 (N) — 8.9 (D) 85 7.8 (D) — 5.5 (D) — 8 (D)
Yang et al. 2021 [76]	Aluminium box Foam Polystyrene	0.95	0.97	—	—	—
Zhang et al. 2021 [75]	Polystyrene foam	0.97	0.81	—	—	6 (D)
Zhou et al. 2021 [73]	Foam box covered with aluminium mylar	0.93	0.87	0	—	4.7 (D) 5 (N) Average: 3.1 (D), 4.2 (N) Average: 2.7 (D), 4.7 (N)
Li et al. 2020 [18]	PMMA shell covered with a layer of aluminium foil Foam	0.96	—	110	—	5 (D) 7 (N)
Zhong et al. 2021 [32]	Foam Polystyrene shell covered with an aluminium foil layer	0.78	0.94	—	—	9 (D)
Zhong et al. 2021 [53]	Aluminium foil	0.90	0.92	—	—	5.4 (D)
Jeong et al. 2020 [62]	Petri dishes	0.97	0.98	—	19.7(D) 14.3(N)	6.2 (D)
Zhang et al. 2020 [21]	Polyurethane board	0.95	0.96	—	90.8	—

doped structures, current simulation methods include Finite-difference-time domain (FDTD) [32] and Mie theory [85].

The above simulation methods can directly use some commercial software or be implemented with self-programmed functions in commercial software. The available commercial software for this purpose are as follows: FDTD can be simulated by Lumerical FDTD [16,23,30,32,39,56,58,65,68,78,79], Comsol Multiphysics [23,34,82] and Essential Macleod [11]; TMM can be simulated in Lumerical FDTD [58]; PSO can be simulated in several script-based tools such as Matlab [29]; Mie theory can be simulated by Lumerical FDTD [39], Matlab [43] and Comsol Multiphysics [82]; Maxwell's equations can be simulated using Lumerical FDTD [58], Comsol Multiphysics [34], and Essential Macleod [11]; and Fresnel's equations can be simulated by Lumerical FDTD [56].

As shown in Table 3, Raman et al. [8] simulated DRCer by Comsol Multiphysics, obtaining a net cooling power of 40 W/m², and an experimental result that was only 0.1 W/m² different than the simulation (measured at 40.1 W/m²). This shows that the theoretical simulation result is in this case accurate when an appropriate mathematical model is selected and representative boundary conditions are set. However, some simulation studies do demonstrate non-negligible errors compared with experimental measurements. For instance, Zhu et al. [11] showed that the simulating cooling temperature drop was 4.3 °C, while the measured value was 3.3 °C in the experiment. The 1 °C difference between the simulation and experimental results was probably caused by inaccurate convective coefficient settings and the sunlight power difference during the experiment and AM1.5 spectral power in simulation. Chae et al. [35] used Matlab to simulate a DRCer and found that the daytime cooling temperature reached 8.3 °C, whereas the experimental daytime ambient temperature was 6.3 °C below ambient. The difference of 2 °C between the simulated and experimental results was probably because the convective heat transfer coefficient (h_c) was

neglected in the simulation.

Overall, Mie theory, Maxwell's equations, and FDTD are commonly used for the design and simulation of DRCers with multilayer and hybrid structures, photonic crystal structures, porous structures, randomly doped structures of polymer nanoparticles, and nanofibre-polymer doped structures. These simulations are used within commercial software, such as Lumerical FDTD, Comsol Multiphysics, Matlab, and Essential Macleod. The simulation results provide a low-cost and highly efficient technique for developing novel DRCers. However, current simulation models and the underlying theory still have some limitations since the accuracy comparisons demonstrate non-negligible differences compared with experimental measurements.

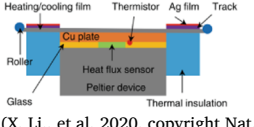
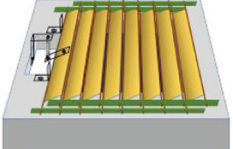
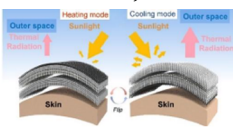
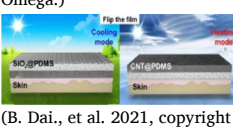
2.3. Manufacturing processes and technologies

Besides the cooling capability of DRCers, the manufacturing process is also one of the crucial factors of its commercial prospects. Table 4 summarizes the fabrication processes and mass production evaluation capability of various DRCers.

In general, polymer-based DRCers, such as the structure of nanoparticles in polymers, porous structure and random nanofibers structure, can be produced by traditional physical and chemical manufacturing methods, i.e. phase inversion method, medium embedding-extracting method, electrospinning method, etc. These DRCers' manufacturing methods are technically mature and low-cost and suited for mass production [88]. Especially, the structure of nanoparticles in polymers [17] and porous structure [16] can be used as painting or coating materials to achieve radiative cooling in buildings. Random nanofibers structure [18] can also be commonly used but it is usually applied in the form of thin films. However, DRCers with these polymer-based porous structures in particular do demonstrate some disadvantages in terms of mechanical properties and fire resistance. To counter these, more research should be

Table 6

Mechanical switchgear for DRCers.

Implementing agency	DRC materials	Switch structure	Switch method	Reference
Actuators & roller	DRC: Polyimide, Ag, PDMS, Heating: Cu, Zn		Rolling by motors	Li et al. 2020 [91]
TSMS	DRC: SiO ₂ , polypropylene, Ag, Cu		1 TCPCS starts to open at 16 °C	Xia et al. 2020 [26]
Flip	DRC: PTFE, PMMA Heating: Nanoporous PE, Zn, Al		Flipping the textile	Luo et al. 2021 [94]
Selvmade shutter	DRC: styrene-ethylene-butylene-styrene and SiO ₂ nanoparticles, Heating: carbon nanotube/polydimethylsiloxane (CNT/PDMS)		The rollers change solar heating and radiative cooling functions side-by-side	Wang et al. 2022 [92]
Flip	DRC: SiO ₂ , PDMS, Heating: CNT, PDMS		Flipping the Janus RC/heating textile film	Dai et al. 2022 [93]

carried out to develop high-performance DRCers with acceptable mechanical properties, with self-healing and refractory cooling materials [88].

On the other hand, the multilayer structure and photonic crystal structure require vacuum vapour deposition [8] and nano-scale lithography [19], which are relatively complex and expensive. Therefore, these two structures are not currently suitable for mass production and large-scale use, even though they have better radiative cooling performance. The manufacturing process of a hybrid structure is a combination of the multilayer structure and other structures. This increases the difficulty and complexity of the manufacturing process and makes mass production more difficult. However, some hybrid structures are not expensive and suitable for mass production as reported in the literatures [58,63,65,67–70]. In conclusion, a balance between energy efficiency and cost should be established for future commercialization of DRCers.

In conclusion, DRCer structures of nanoparticles in polymers, porous structures and random nanofibers structures, can be manufactured by traditional physical and chemical manufacturing methods. This means these structures are technically mature, less costly and suitable for mass production. Meanwhile, the structure of nanoparticles in polymers and the porous structure can be used as radiation-cooled coatings and paintings for energy-efficiency purposes in building applications, while random nanofibers structure is often available in the form of thin films. On the other hand, the multilayer structure, photonic crystal structure and hybrid structures require vacuum vapor deposition and nanoscale lithography, which is a complex and expensive manufacturing process and is not currently suitable for mass production and large-scale use.

2.4. Insulation and cover materials for DRCers experiments

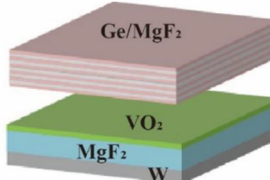
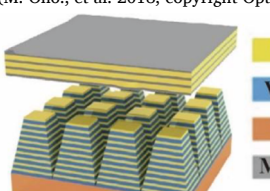
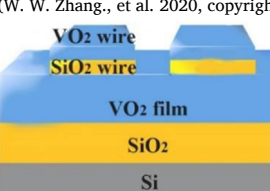
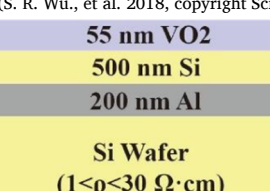
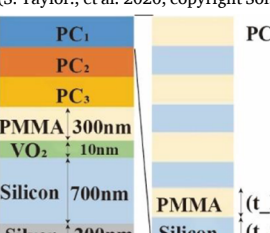
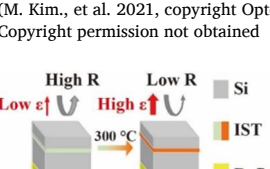
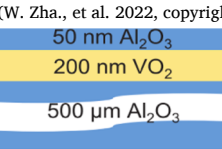
Insulation and cover materials are of vital importance to improve the performance of DRCers since they can reduce heat loss to the ambient. The cover shields include non-selective covers and selective covers. The non-selective cover would be able to allow transmission at almost all wavelengths, and the selective covers can prevent the beneath emitter from heating up due to solar radiation while allowing MIR thermal radiation to pass through [89].

PE is the most representative non-selective cover shield [6,8,12,17,18,20–22,29,30,32,34–40,43,44,49,53,59,62,63,65,67,69,70,72,73,75,76,78,79,81–84,90], and its transmittance is affected by its thickness. PE has high transmittance over almost the entire spectrum except the absorption peaks at 3.4, 3.5, 6.8, 7.3, 13.7, and 13.9 μm [47] which are far away from the “atmospheric window”. Both types of PE (high-density polyethylene (HDPE) and low-density polyethylene (LDPE)) can be used as cover shields. However, the HDPE is harder with better mechanical strength, while the LDPE has better optical performance in comparison [89]. Therefore, the inexpensive PE is widely used for various experiments in daytime radiative cooling experiments [47].

However, the spectral selectivity for selective cover remains to be a challenge due to stringent requirements of low transmissivity in the solar spectrum and high transmissivity in the “atmospheric window” [89]. Selective cover materials usually appear in the form of coatings with high reflectance characteristics in 0.2–3 μm [89]. There are two types of selective cover materials: one has high transmittance in 8–13 μm (up to 0.95 [89]), such as ZnSe [33] and ZnS [47] coatings; the other has high absorption in 8–13 μm (up to 0.30–0.95 [89]), such as ZnO [47], TiO₂ [47] and ZrO₂ [47] coatings. Compared with non-selective

Table 7

TADRCers with non-volatile phase-change materials layers.

Materials	Structure	Switching material	Switch temperature	Reference & Author
VO ₂ , MgF ₂ , W, Ge, MgF ₂	 (M. Ono., et al. 2018, copyright Opt. Express.)	Co-doping of W and Sr to pure VO ₂	10–25 °C	Ono et al. 2018 [27]
Ge, VO ₂ , Ti, MgF ₂	 (W. W. Zhang., et al. 2020, copyright Opt. Express.)	VO ₂	68 °C	Zhang et al. 2020 [105]
VO ₂ , SiO ₂ , VO ₂ , Si	 (S. R. Wu., et al. 2018, copyright Sci Rep.)	VO ₂	68 °C	Wu et al. 2018 [28]
VO ₂ , Si, Al	 (S. Taylor., et al. 2020, copyright Sol. Energy Mater. Sol. Cells)	VO ₂	65–75 °C	Taylor et al. 2020 [108]
PMMA, Si, VO ₂		VO ₂	68 °C	Kim et al. 2021 [109]
Polyimide, Si, WVO ₂ , BaF ₂ , Ag IST, SiO ₂ , Ti, Au, Si	 (M. Kim., et al. 2021, copyright Opto-electron. Adv.) Copyright permission not obtained	WxV1-xO ₂ IST	22 °C 250 °C	Tang et al. 2021 [110] Zha et al. 2022 [103]
Al ₂ O ₃ , VO ₂ , Al	 (W. Zha., et al. 2022, copyright ACS Photonics.) (X. Ao., et al. 2022, copyright Proc Natl Acad Sci U S A.)	VO ₂	63.7–67.9 °C	Ao et al. 2022 [111]

(continued on next page)

Table 7 (continued)

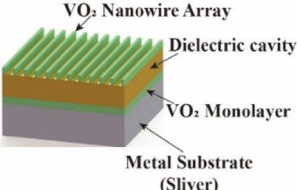
Materials	Structure	Switching material	Switch temperature	Reference & Author
BaF ₂ , VO ₂ , Ag	 (K. Araki, R., et al. 2022, copyright Int. J. Heat Mass Transf.)	VO ₂	68 °C	Araki et al. 2022 [112]

Table 8Phase change temperature and optical properties of VO₂ doped materials.

Materials	Switch temperature	τ_{UV-VIS} and corresponding temperature	τ_{MIR} and corresponding temperature	Reference
Poly(ethyleneimine), silver nitrate, ethanol absolute, W + VO ₂	20 ~ 45 °C	0.75 (20 °C) 0.50 (45 °C)	–	Meng et al. 2022 [115]
W (1.5%) + VO ₂ , HfO ₂ , H ₂ O	20 ~ 80 °C	0.70 (25 °C) 0.10 (90 °C)	–	Xu et al. 2019 [118]
VO ₂ + Fe (0~9.2%) + Mg (0~11.9%)	20 ~ 90 °C	0.74 (20 °C) 0.15 (90 °C)	–	Ji et al. 2018 [116]
Doping VO ₂ coatings with tungsten, fluorine, gold nanoparticles	20 ~ 100 °C	0.20 ≤ τ_{VIS} ≤ 0.78 (Below 20~25 °C) 0.20 ≤ τ_{VIS} ≤ 0.74 (Above 65~100 °C)	0.19 ≤ τ_{MIR} ≤ 0.80 (Below 20~25 °C) 0.03 ≤ $\tau_{infrared}$ ≤ 0.50 (Above 65~100 °C)	Kamalisarvestani et al. 2013 [119]
VO ₂ + ITO (1%, 7.5%)	30 ~ 70 °C	0.99 (30 °C) 0.60 (70 °C)	0.98 (30 °C) 0.30 (70 °C)	Ono et al. 2021 [114]
VO ₂ + SnO ₂	30 ~ 90 °C	0.77 (30 °C) 0.15 (90 °C)	–	Liu et al. 2021 [120]
W + VO ₂ (W/V = 0~1.63%)	32 °C	–	0.1 (20 °C) 0.99 (90 °C)	Sun et al. 2022 [121]
VO ₂ + ITO + TiO ₂	52 °C	–	0.45~0.65 (25 °C) 0.25~0.60 (85 °C)	Miller et al. 2016 [122]
VO ₂ + TiO ₂	61.5 °C	–	0.75 (25 °C) 0.25 (90 °C)	Zheng et al. 2015 [123]
VO ₂ + SiO ₂ + TiO ₂	69.3 °C	–	0.70 (\geq 69.3 °C) 0.19 (\leq 69.3 °C)	Sol et al. 2020 [124]
VO ₂ + sapphire (Al ₂ O ₃)	66.8 °C	–	–	Liu et al. 2012 [117]

covers, selective coverings have better durability, but the raw materials are more expensive and the optical properties need to be further improved [47,89].

The insulation for the DRCers consists of a frame material and a surface reflective material, see Table 5. The frame materials include wood frame, PMMA, polystyrene, Polystyrene foam, Polyvinyl chloride, etc. These materials serve to reduce the conduction of heat transfer with the surrounding environment. To prevent solar radiation heating the insulation materials and the DRCers cooling space, highly reflectivity film materials, such as aluminium mylar [20], aluminium foil [70] and silver layer [49] are needed to be added to the surface of the frame. In addition, vacuum insulation gaps can be used to prevent convection heat transfer, e.g. Chen et al. [33] placed a DRCer in a vacuum chamber and showed a daylight temperature drop of 42.2 °C. This far exceeds other literature on daytime cooling temperatures, but the application scenario is limited and the experimental cost is high.

From the above it was found that cover materials and insulation materials (i.e. wood frame, PMMA, polystyrene, polystyrene foam, polyvinyl chloride, vacuum gaps) with highly reflective film layers (i.e. aluminium mylar, aluminium foil or silver layer) improve DRCers' performance, because they can reduce heat loss to the ambient environment. Polyethylene is the most commonly used non-selective material for cover shields. On the other hand, the selective cover remains a challenge because of stringent requirements at different wavelengths. ZnSe, ZnS, ZnO, TiO₂, and ZrO₂ coatings are often used as selective cover materials.

3. Current situation and prospects of DRCers control technology

3.1. Mechanical switches for DRCers

3.1.1. Mechanical switchgear

As summarized in Table 6, mechanical switchgear can be installed with DRCers to switch-on or switch-off thermal radiation depending on the ambient temperature, which could change P_{rad} or/and P_{sun} to turn on/off radiative cooling. There are several types of mechanical switchgear for DRCers applications: integrate a baffle with the mechanical actuator and the temperature feedback controller and install it above the DRCer (Xia et al. 2020 [26]); or use a mechanical switching device (Li et al. 2020 [91]) or manual switching device (Wang et al. 2022 [92]) to flip a DRCer with radiative cooling on one side and heat absorption or insulation on the other, as shown in Table 6.

In 2020, Xia et al. [26] used a temperature shape memory spring (TSMS) as the temperature switch feedback with an actuator mounted on the temperature-controlled phase change structure (TCPSCS) to uncover or shield the DRCer. When the ambient temperature is below 16 °C, to prevent radiative cooling, the TCPSCS sheet is in a horizontal position to block the radiative heat transfer from the DRCer to the outer space. Conversely, when the ambient temperature is over 20 °C, the thin TCPSCS sheet moves in a vertical or diagonal open position and radiative cooling is reactivated. The average all-day temperature of DRCer decreased by 2.2 °C when TCPSCS was switched off, but the temperature decreased by 5.9 °C for the same DRCer without TCPSCS on the same

Table 9

Summary of thermo-colour changing materials.

Materials	Switch temperature	Colour, τ_{UV-VIS} and corresponding temperature	τ_{MIR} and corresponding temperature	Reference
Hydroxypropyl cellulose, dimethyl sulfoxide, ITO	20 ~ 40 °C	–	–	Wang et al. 2021 [140]
Poly (N-isopropylacrylamide) hydrogel and polyvinylidene fluoride	31 °C	–	–	Mei et al. 2022 [141]
The N-isopropylacrylamide monomer, N,N0-methylenebis(acryla-mide) crosslinker, ammonium persulfate initiator, Sodium dodecyl sulfate surfactant, and 2-Aminoethylmethacrylate hydrochloride monomer	25 ~ 35 °C	0.87 (22 °C) 0 (40 °C)	–	Li et al. 2019 [142]
N-isopropylacrylamide, N,N-methylenebis (acrylamide), N,N,N,N-tetramethylethylenediamine, ammoniumperoxydisulfate	20 ~ 60 °C	–	0.90 (20 °C) 0.05 (60 °C)	Zhou et al. 2020 [143]
Sodium acetate, PDMS	40 ~ 60 °C	0.78 (20 °C) 0.4 (50 °C)	–	Cho et al. 2019 [145]
Monodisperse silica particles with distinct sizes (100 nm, 300 nm, 500 nm, 1 μm, 2 μm, 3 μm, and 5 μm), aluminum	78.3 °C	0.11 (<63.3 °C) 0.94 (\geq 78.3 °C)	–	Zhang et al. 2022 [144]
LEXANTM 8040 T PC films and a benzophenone-PC copolymer films, Liquid crystalline monomers, benzophenone dye 5 and potassium hydroxide pellets, the surfactant	5 ~ 15 °C	0.68 (5 °C) 0.92 (30 °C)	0.95 (5 °C) 0.63 (30 °C)	Ellen P. A et al. 2019 [146]
Nematic liquid crystal and R-form chiral dopant	27 ~ 75 °C	27 °C: Red 82 °C: Yellow	–	Lee et al. 2017 [147]

day's experiment. The experimental results indicated that the integrated TCPCS into DCRes does achieve the switching effect. Li et al. [91] demonstrated a heating and cooling dual-mode motor switching device. The cooling surface has 0.97 reflectivity in 0.3–2 μm and 0.94 emissivity in 8–13 μm. The heating surface has 0.93 absorption in 0.3–2 μm and 0.14 emissivity in the MIR. When switching to the cooling surface, the net cooling power reached 71.6 W/m² at a daylight power of 643.4 W/m². On the contrary, when turning on the solar heating surface P_{sun} would increase and P_{rad} would decrease.

In 2022, Wang et al. [92] developed a dual-mode superhydrophobic film which consists of porous coating of styrene-ethylene-butylene-styrene/SiO₂ for radiative cooling and nanocomposite coating of carbon nanotubes/polydimethylsiloxane for solar heating. In the cooling mode, the film achieved sunlight reflection of 0.94 and emission of 0.92 in MIR and contributed to 11 °C temperature drop. In the heating mode, the film achieved solar absorption of 0.98 and raised the air temperature by up to 35.6 °C.

The above mechanical switch with temperature feedback system [26] and manual mechanical switches [91–93] could switch-on and switch-off the DRC. However, manual operation switches need further integration with automatic control systems to be able to switch on/off frequently according to ambient conditions. In addition, a mechanical switch actuator with a temperature feedback system is complex, bulky [26,91], difficult to manufacture and has high maintenance costs. These disadvantages limit its large-scale application.

3.1.2. Elastomeric modulator

An Elastomeric modulator is made from elastomeric optical materials, which can change its reflectivity and emissivity by changing its stretching state. For instance, Fang et al [95] demonstrated a device that comprises a surface-textured infrared-semi-absorbing elastomer coated with a metallic back reflector, which is biaxially strained to sequentially achieve three fundamental modes: In emission mode, the modulator has the highest emittance of 0.78 ± 0.01 and a low transmittance of ~ 0.01 ; In reflection mode, the reflectance of 0.60 ± 0.01 dominates, and the transmittance becomes $\sim 0.03 \pm 0.01$; In transmission mode, the film transmittance rises to 0.52 ± 0.02 , while the reflectance and absorptance decrease to 0.28 ± 0.02 and 0.20 ± 0.01 respectively. Li et al. [96] reported an analysis of optical transmittance polydimethylsiloxane (PDMS) films which can be tuned up between transmittance of 92% and 9.2% with moderate 0–50% uniaxial tensile strain.

Elastomeric modulators showed potential for DRC switching applications. However, the tension and release of the elastomeric modulator

material require an external force, for example with a switching actuator. This means to achieve temperature switching, the elastomeric modulator needs to integrate mechanical actuators or temperature-adaptive shape memory materials. The ageing resistance of elastomeric modulators also needs further investigation.

3.1.3. Temperature-adaptive shape memory polymers (TSMPs) switch

Temperature-adaptive shape memory polymer (TSMP) switches can change their shape in response to the ambient temperature. Therefore, integrating TSMPs with DRCers can form TADRCers that keep DRC switch-on or switch-off in different ambient temperatures. Liu et al. [97] fabricated a thermal responsive structure by 3D printing for environmentally adaptive cooling and heating. The transition between open and close states occurred at 32 °C within a minute, resulting in a 0.35 emissivity difference and 22 W/m² power difference between open and close states. Zhang et al. [98] developed a TADRCer by integrating a reversible temperature-sensitive shape memory material layer which is made of polytetrahydrofuran, polycaprolactone, hexamethylene diisocyanate and dibutyltin dilaurate. The switching temperature was in the range of 23–24 °C and the unit had an average solar heating power and radiant cooling power of 859.8 W/m² and 126.0 W/m², respectively.

Other TSMP materials with similar properties also have the potential to integrate into DRC. For instance, Li et al. [99] prepared the butterfly-wing-like smart window composed of PDMS and polyurethane with a deformable surface morphology inherited from a TSMP. The τ_{UV-VIS} is 0.68 when the ambient temperature is above 45 °C and this value is decreased to 0.25 when the temperature is below 45 °C.

Shape memory polymers (SMPs) as a smart material are highlighted by many researchers since they show the advantages of being lightweight and having a larger deformed ability, controllability, and tunable performance [100–102]. The switching process of TSMPs is passive and does not require energy use [98].

Overall, the mechanical switchgear, elastomeric modulators and TSMPs were reviewed and compared. The mechanical switching control system is sensitive, and the switching temperature can be set flexibly, but the system's limitations are complexity, durability and high cost. The elastomeric modulator structure showed potential in being applied for DRCer control, but it requires an external force to be added for switching. The TSMPs in DRCer's switch accessories have the advantages of being lightweight, have controllable performance, large deformation and strong structural design, but their actuator is complex and bulky.

3.2. Temperature adaptive switching materials

3.2.1. Non-volatile phase change materials

The non-volatile phase change materials (PCMs) (i.e. VO₂ [27] and In₃SbTe₂ (IST) [103]) can be used for tunable nanophotonic devices due to their high dielectric optical contrast between the amorphous and crystalline structural phases [104]. There are two kinds of methods to combine non-volatile PCM with DRCer as a TADRCer: (1) the non-volatile PCM layer is used as a selective cover, as shown by Masashi et al. [27] and Zhang et al. [105]; (2) Combining the non-volatile PCM layer, emission layer and reflection layer as a TADRCer by Wu et al. [28], as shown in Table 7.

VO₂ is at a transmissive insulating phase when its temperature is below 68 °C [28,105,106]. To this end, DRCers containing a VO₂ switch layer show low emissivity in “atmospheric window” [107], which would reduce P_{rad}. On the other hand, VO₂ has a metallic phase when its temperature is above 68 °C, which would increase the emissivity and the P_{rad} of a DRCer. Therefore, integrating VO₂ into a DRCer would be able to adjust the magnitude of P_{rad} to achieve a self-switching response to the ambient temperature. For example, Ono et al. [27] undertook a theoretical evaluation of a temperature self-adaptive radiative cooling system based on a planar photonic multilayer system incorporating VO₂ and a spectrally selective filter which can automatically turn off radiative cooling when the temperature is below the transition temperature of VO₂. Wu et al. [28] proposed a tunable MIR metasurface VO₂/SiO₂/VO₂ cavity structure whose theoretical cooling power density in the turn-on state is fourfold as the device temperature is below the phase change temperature of VO₂. Taylor et al. [108] fabricated a VO₂-based tunable metafilm emitter, and the total emittance change of over 0.45 had been displayed by the fabricated emitter during experiments. In 2022, Zhang et al. [105] composed of a top filter and a periodic trapezoidal VO₂-Ge multilayer absorber which has very different emittance in the 8–13 μm band at different temperatures.

IST is a switchable infrared plasmonic PCM whose optical properties change from dielectric to metallic upon crystallization in the whole infrared spectral range [103]. This property allows the optical parameters and emissivity (P_{rad}) to be altered at a phase change temperature of 300 °C [103]. For example, Zha et al. [103] proposed two nonvolatile high-contrast switchable IST emitters: One switchable emitter exhibits negative differential emissivity and is applied as a barrier to infrared radiation; the other one shows positive differential and demonstrates capability in thermal management.

However, the VO₂ phase change temperature (68 °C) is too high for switching radiative cooling in buildings [113]. Therefore, some researchers studied doping Sn-doped In₂O₃ (ITO) [114], tungsten (W) [115], strontium (Si) [109], iron (Fe) [116], Magnesium (Mg) [116] and metal oxides [117] into VO₂ to adjust phase transition temperature to 20–100 °C. The application of the resulting materials in TADRCers are shown in Table 8. For instance, the temperature decreased from 68 °C to 20 ~ 45 °C after being doped with W [115]. However, VO₂-based materials have some limitations, for example, VO₂ doping with these materials is relatively expensive and complex in photolithography processing, and the absorption rates of VO₂-based materials for solar radiation are non-negligible. It is therefore difficult to use these materials for large-scale production and application in TADRCers.

Temperature-adaptive switching materials have the advantages of adaptive passive control, easy integration into DCRer, and temperature sensitivity. The switching temperature of VO₂ is 68 °C, and this temperature limits its application in the field of building energy saving. The same conclusion applies to In₃SbTe₂, which has a switching temperature of 250 °C. Although the switching temperature of VO₂ can be conditioned by the addition of other elements and can range between 10 and 100 °C, both the VO₂ material itself and the element-doped VO₂ are still too expensive for large-scale applications.

3.2.2. Paraffin waxes

The phase change paraffin (n-alkane) has a significant transmittance difference between liquid and solid phases. Liquid paraffin has a transmittance of over 0.90 in both the UV-VIS and mid-infrared bands [125,126], while in the solid state the transmittance is less than 0.05 [125,127]. The phase change temperature of paraffin waxes (alkanes) is in the range of –12 to 75.9 °C [113]. Goia et al. [128] designed optical smart windows with paraffin that simultaneously meet the requirements of daytime illumination, absorption of infrared radiation, thermal storage and energy conservation in buildings. Kim et al. [129] designed phase change lenses with octadecane and used it as a thermal switch and thermal storage material in solar thermoelectric systems. Meanwhile, doping of metal oxide particles (e.g. ZnO or CuO) into paraffin can adjust its transmittance [130]. Therefore, paraffin can be used as a raw material for the development of transmissive switch film [127] as a DRCer cover. At the same time, paraffin has the characteristics of safety, non-toxicity, non-corrosiveness and low cost [113]. Therefore, paraffin as a raw material for the design of transmissive switching sheets can be combined with a DRCer to form a TADRCer. The solid paraffin film prevents the DRCer’s emitter heat transfer and absorbs sunlight. Otherwise, paraffin in a liquid state with high transmittance might result in a P_{net-cooling} larger than zero.

Form-stabilized PCM (FSPCM) composed of paraffin and carrier material (e.g. PDMS) can maintain its macroscopic solid form [106,131,132] even after paraffin has melted. FSPCM enables a temperature-adaptive optical switching function [127]. For example, Shi et al. [133] successfully made 0.1–8 mm thick FSPCM with 0–30 w.t. % of paraffin in PDMS as an optical switching material. Apostoleris et al. [134] produced 1.3 mm thick FSPCM films with paraffin content of 2 w.t.%, 10 w.t.% and 20 w.t.% in PDMS and with a phase transition temperature between 44 and 46 °C. Results showed that the average UV-VIS transmittance exceeds 0.90 while the film was switched-on. On the contrary, the average UV-VIS transmittance was less than 0.70 during the switch-off state. Zhang et al. [135] produced FSPCM with paraffin content of 1 w.t.%, 2 w.t.%, 3 w.t.%, 4 w.t.% and 5 w.t.% in PDMS and analyzed the surface morphology by an Atomic Force Microscope. The films can be switched from opaque to transparent for temperatures above 53 °C. Su et al. [127] produced FSPCM films within the 10–30 w.t. % paraffin range in PDMS, i.e. OCT10%, OCT20% and OCT30%. The UV-VIS and FTIR testing results showed a significant switching effect during the solid-liquid phase at UV-VIS and MIR wavelengths. The solidification temperatures for OCT10%, OCT20% and OCT30% were 24.9 °C, 25.9 °C and 25.1 °C, respectively. The phase change temperature differences between the solidification and melting of these films were much smaller than VO₂ doped materials, which means that the paraffin based FSPCMs’ thermal response sensitivity is higher. Meanwhile, the films also showed high emissivity in 8–13 μm, which showed a potential for their use in the development of TADRCers. Su et al. [136] further developed a spectrally self-switchable cover by three layers of PE-PCM-PE films and provided a new solution for achieving TADRC. However, the average transmittance of this cover was only 40% in the atmospheric window when the cover was composed of two layers of 100 μm PE and a 300 μm PCM layer. Therefore, it was necessary to reduce the thickness of PE and PCM layers to optimize the cover performance.

The phase change paraffin (n-alkane) has a transmittance of over 90% in both the UV-VIS and MIR bands, while in the solid state the transmittance is less than 5%. The phase change temperature range of paraffin is –12 to 75.9 °C, depending on its carbon chain length. Paraffin waxes exhibit advantages of safety, non-toxicity, non-corrosiveness, and low cost. However, it is necessary to use a carrier material to fabricate a form-stabilized PCM to overcome the leakage problem of PCM in TADRCers.

3.2.3. Thermo-chromic materials

Thermo-colour-changing materials have the potential to be used as a temperature-adaptive switch for TADRCers, as summarised in Table 9.

Usually, colour-changing materials can respond to electro-, thermo-, mechano- and photo-chromic signals [137]. Among them, thermo-chromic materials integrated with DRCers may achieve the adaptive switching effect of radiative cooling due to their varying optical properties that could result in different P_{rad} and P_{sun} at different ambient temperatures [137,138].

Thermo-chromic hydrogels in particular are polymer networks that undergo a hydrophilic and hydrophobic phase transition at different temperatures[106,139]. For example, Wang et al. [140] used Hydroxypropyl cellulose, dimethyl sulfoxide and ITO as raw materials to develop temperature-adaptive radiative cooling smart windows, which can automatically switch-on and switch-off radiative cooling between 20 and 40 °C. When the ambient was above the switching temperature, the smart windows could achieve temperatures 5.4 °C below the normal glass. In the remaining time, the smart window can switch off the cooling mode and its temperature was 4.5 °C above the normal glass. Compared to other control methods, the temperature-adaptive radiative cooling smart windows with thermo-chromic hydrogels are relatively cheap and are therefore particularly suitable for TADRCer applications in low-carbon buildings. Mei et al. [141] designed a temperature self-adaptive sandwich structure film based on a thermo-chromic poly(N-isopropylacrylamide) hydrogel and polyvinylidene fluoride film. The film achieved a cooling effect of 1.8 °C when its temperature was above 31 °C. When radiative cooling was closed, the film's temperature was 5.8 °C higher than the ambient temperature.

Other thermo-chromic hydrogels also showed temperature-switching properties, although they have not been applied in TADRCers, as shown in Table 9. For instance, Li et al. [142] produced a smart window using N-isopropylacrylamide monomer (NIPAm, 98%), N,N-methylenebis (acryla-mide) (BIS, 99%) crosslinker, ammonium persulfate (R98%) initiator, SDS (R98.5%) surfactant, and 2-Aminoethylmethacrylate hydrochloride monomer (AEMA, 95%) as raw materials. When the ambient temperature is 22 °C, the $\tau_{\text{UV-VIS}}$ is approximately 0.87. However, the $\tau_{\text{UV-VIS}}$ is close to 0 when the ambient temperature is 40 °C and therefore the P_{sun} at 40 °C is less than the P_{sun} at 22 °C. This makes the P_{rad} at high ambient temperatures greater than the P_{rad} at low ambient temperatures if applying this smart window to a DRCer. In addition, Zhou et al. [143] used N-isopropylacrylamide, N,N-methylenebis (acrylamide), N,N,N,N-tetra- methylethylenediamine, ammoniumperoxydisulfate as materials to prepare smart windows. The switching temperature range in Zhou et al.'s study was 25–60 °C. The τ_{MIR} was about 0.90 at an ambient temperature of 20 °C and close to 0.05 at an ambient temperature of 60 °C. Unlike Li et al. [142], the switch in Zhou et al. [143] could change the P_{rad} by controlling the τ_{MIR} .

The production process of thermo-chromic hydrogels is relatively simple and their switching temperature is in the range of 20–60 °C, which makes it possible to be used as a temperature switch for TADRCers. In addition, hydrogel materials have been reported to further enhance the radiative cooling power by up to 150 W/m² through additional evaporative cooling [88]. However, solvent leakage problems pose some limitations to their further commercial application.

Other non-hydrogel thermo-chromic materials in Table 9 also can change their emissivity and reflectance in response to the ambient temperature and show temperature-switching properties. For example, Zhang et al. [144] developed a thermal adaptive switchable radiation cooling device using a porous silica coating with liquid separation/incorporation carbon tetrachloride matched to the refractive index. The solar transmittance of this device was only 0.11 in opaque mode (temperature rise of 10 °C in winter) and 0.94 in transparent mode (temperature drop of 5 °C in summer), which allowed for a complete switching process within 3 min for over 500 switching iterations.

Thermo-chromic hydrogels can also be used for temperature-switching purposes in TADRCers with their switch temperatures being in the range of 20–60 °C. In addition, the production process of thermo-chromic hydrogels is relatively simple and could enhance the radiative cooling power through additional evaporative cooling. The review also

included other types of thermo-chromic materials that can be theoretically integrated with DRCers to achieve the adaptive switching effect of radiative cooling. Overall, passive response switching materials do not require complex control systems, they are easy to use and have low maintenance costs.

4. Conclusions and outlook

This paper provides a comprehensive and critical review of static DRCers /TADRCers and related TADRCers' control technologies and mechanisms. Generally, static DRCers are unable to automatically turn on and off radiative cooling in response to ambient temperature changes. Therefore, in most climates, retrofitting the existing static DRCers to TADRCers would be essential to ensure DRCers do not impose a heating penalty in buildings during winter.

According to the review of structures, materials, manufacturing and experimental methods and performance outputs, DRCer demonstrated better cooling performance when the solar reflectance and MIR emissivity is high. When experiments were undertaken during low solar radiation and high atmospheric transmittance periods, DRCers would typically show a better daytime cooling performance. DRCer structures of nanoparticles in polymers, porous and random nanofibers structures are technically mature, less costly and suitable for mass production. In most cases, the structure of nanoparticles in polymers and the porous structure can be used as radiative cooling coatings and paintings for energy-efficiency purposes in buildings. Meanwhile, Mie theory, Maxwell's equations, and FDTD are commonly employed for designing and simulating various DRCer structures by commercial software, i.e. Lumerical FDTD, Comsol Multiphysics, Matlab and Essential Macleod.

Current control technologies for TADRCers include mechanical switchgear, elastomeric modulators, temperature-sensitive material mechanical switches and DRCer integrated with some temperature-adaptive optical switching materials, i.e. VO₂ and In₃SbTe₂. Compared with temperature-adaptive optical switching materials, the mechanical switches are sensitive, and offer flexibility in setting the switching temperature, but their disadvantages are complexity, durability and high cost. On the other hand, the switching temperature of VO₂ and In₃SbTe₂ (optical switching materials) is much higher than the typical temperature required for energy-saving applications in buildings. The phase change paraffin waxes are identified as a viable option for switching materials due to the large transmittance difference in solid and liquid phases in the UV–VIS and MIR bands, and exhibit advantages of safety, non-toxicity, non-corrosiveness and low cost. However, for paraffin waxes, it is necessary to overcome the leakage issues during the melting phase. Thermo-chromic hydrogels are also considered as temperature-switching materials with potentially additional evaporative cooling potential.

In conclusion, future work should focus on the development of DRCers with the structure of nanoparticles in polymers, porous structure and random nanofibers structure. It is also essential to develop industry standard manufacturing processes for DRC materials, especially for the application of DRC materials as paintings for energy-efficient buildings. Meanwhile, the mechanical durability and fire protection properties of these polymer-based DRC materials require improvements and further study. For the seasonal application of DRC, temperature-adaptive properties are necessary and static DRCers should be retrofitted to TADRCers. Based on the above review, we believe that under the condition of solving the cost and manufacturing difficulty of temperature-adaptive switching materials, they have more practical value than the use of mechanical switches. In the longer term, we believe temperature-adaptive daytime radiative coolers present the ultimate embodiment of DRCer, enabling all-season thermal regulation, being highly efficient and having low-cost module manufacturing and wider deployment.

CRediT authorship contribution statement

Weiguang Su: Writing – original draft, Validation, Supervision, Investigation, Funding acquisition, Formal analysis, Conceptualization. **Pei Cai:** Writing – original draft, Visualization, Investigation, Data curation. **Jo Darkwa:** Writing – review & editing, Funding acquisition. **Mingke Hu:** Writing – review & editing. **Georgios Kokogiannakis:** Writing – review & editing. **Chonghai Xu:** Writing – review & editing. **Li Wang:** Writing – review & editing, Funding acquisition.

Declaration of Competing Interest

The authors declare that they have no known competing financial interests or personal relationships that could have appeared to influence the work reported in this paper.

Data availability

No data was used for the research described in the article.

Acknowledgements

Weiguang Su thanks the support of Qing Chuang Plan by Shandong Province Department of Education (Sub-Title: Innovative Research Team of Advanced Energy Equipment) and National Natural Science Foundation of China (NSFC) (No. 51908299); Li Wang thanks the support by Jinan Scientific Research Leader Studio (No. 2021GXRC083) and Science, Education and Industry Integration Innovation Pilot Project from Qilu University of Technology (Shandong Academy of Sciences) (No.2022JBZ02-01); Jo Darkwa thanks the support by UK Engineering, Physical Sciences Research Council (EPSRC) (under Grant Award No. EP/V041452/1). We acknowledge the copyright permission from the journals for the graphics, images, and figures.

References

- [1] D.K. Bhamare, M.K. Rathod, J. Banerjee, Passive cooling techniques for building and their applicability in different climatic zones—the state of art, *Energ. Buildings* 198 (2019) 467–490, <https://doi.org/10.1016/j.enbuild.2019.06.023>.
- [2] N. Santillán-Soto, O. García-Cueto, A. Lambert-Arista, S. Ojeda-Benítez, S. Cruz-Sotelo, Comparative Analysis of Two Urban Microclimates: Energy Consumption and Greenhouse Gas Emissions, *Sustainability*. 11 (2019) 2045, <https://doi.org/10.3390/su11072045>.
- [3] S.K. Singh, S. Sundaram, K. Kishor, *Photosynthetic Microorganisms Mechanism For Carbon Concentration* (2014).
- [4] F. Ascione, Energy conservation and renewable technologies for buildings to face the impact of the climate change and minimize the use of cooling, *Sol. Energy* 154 (2017) 34–100, <https://doi.org/10.1016/j.solener.2017.01.022>.
- [5] Y. Yang, Y. Zhang, Passive daytime radiative cooling: Principle, application, and economic analysis, *MRS Energy & Sustainability*. 7 (2020), <https://doi.org/10.1557/mre.2020.18>.
- [6] T. Suichi, A. Ishikawa, Y. Hayashi, K. Tsuruta, Performance limit of daytime radiative cooling in warm humid environment, *AIP Adv.* 8 (2018), 055124, <https://doi.org/10.1063/1.5030156>.
- [7] E. Rephaeli, A. Raman, S. Fan, Ultrabroadband photonic structures to achieve high-performance daytime radiative cooling, *Nano Lett.* 13 (2013) 1457–1461, <https://doi.org/10.1021/nl4004283>.
- [8] A.P. Raman, M.A. Anoma, L. Zhu, E. Rephaeli, S. Fan, Passive radiative cooling below ambient air temperature under direct sunlight, *Nature* 515 (2014) 540–544, <https://doi.org/10.1038/nature13883>.
- [9] P. Yang, C. Chen, Z.M. Zhang, A dual-layer structure with record-high solar reflectance for daytime radiative cooling, *Sol. Energy* 169 (2018) 316–324, <https://doi.org/10.1016/j.solener.2018.04.031>.
- [10] M. Hu, G. Pei, Q. Wang, J. Li, Y. Wang, J. Ji, Field test and preliminary analysis of a combined diurnal solar heating and nocturnal radiative cooling system, *Appl. Energy* 179 (2016) 899–908, <https://doi.org/10.1016/j.apenergy.2016.07.066>.
- [11] Y. Zhu, Y. Ye, D. Wang, Y. Cao, Simple dual-layer emitter for daytime radiative cooling, *OSA Continuum.* 4 (2021) 416–427, <https://doi.org/10.1364/OSAC.398685>.
- [12] J.-I. Kou, Z. Jurado, Z. Chen, S. Fan, A.J. Minnich, Daytime Radiative Cooling Using Near-Black Infrared Emitters, *ACS Photonics* 4 (2017) 626–630, <https://doi.org/10.1021/acspophotonics.6b00991>.
- [13] M.M. Hossain, M. Gu, Radiative Cooling: Principles, Progress, and Potentials, *Adv. Sci. (Weinh.)*. 3 (2016) 1500360, <https://doi.org/10.1002/advs.201500360>.
- [14] A. Mohammed, S. Yesudas, S. Chacko, A multilayered photonic emitter for high-performance daytime radiative cooling, *Microsyst. Technol.* 27 (2020) 2873–2887, <https://doi.org/10.1007/s00542-020-05091-2>.
- [15] B. Ko, D. Lee, T. Badloe, J. Rho, Metamaterial-Based Radiative Cooling: Towards Energy-Free All-Day Cooling, *Energies* 12 (2018) 89, <https://doi.org/10.3390/en12010089>.
- [16] J. Mandal, Y. Fu, A.C. Overvig, M. Jia, K. Sun, N.N. Shi, et al., Hierarchically porous polymer coatings for highly efficient passive daytime radiative cooling, *Science* 362 (2018) 315–319, <https://doi.org/10.1126/science.aat9513>.
- [17] X. Li, J. Peoples, Z. Huang, Z. Zhao, J. Qiu, X. Ruan, Full Daytime Sub-ambient Radiative Cooling with High Figure of Merit in Commercial-like Paints, *Cell Reports Physical Science.* 1 (2020), 100221, <https://doi.org/10.1016/j.xcrp.2020.100221>.
- [18] D. Li, X. Liu, W. Li, Z. Lin, B. Zhu, Z. Li, et al., Scalable and hierarchically designed polymer film as a selective thermal emitter for high-performance all-day radiative cooling, *Nat. Nanotechnol.* 16 (2020) 153–158, <https://doi.org/10.1038/s41565-020-00800-4>.
- [19] M.M. Hossain, B. Jia, M. Gu, A Metamaterial Emitter for Highly Efficient Radiative Cooling, *Adv. Opt. Mater.* 3 (2015) 1047–1051, <https://doi.org/10.1002/adom.201500119>.
- [20] H. Zhong, P. Zhang, Y. Li, X. Yang, Y. Zhao, Z. Wang, Highly Solar-Reflective Structures for Daytime Radiative Cooling under High Humidity, *ACS Appl. Mater. Interfaces* 12 (2020) 51409–51417, <https://doi.org/10.1021/acsami.0c14075>.
- [21] H. Zhang, K.C.S. Ly, X. Liu, Z. Chen, M. Yan, Z. Wu, et al., Biologically inspired flexible photonic films for efficient passive radiative cooling, *PNAS* 117 (2020) 14657–14666, <https://doi.org/10.1073/pnas.2001802117>.
- [22] Y. Zhai, Y. Ma, S.N. David, D. Zhao, R. Lou, G. Tan, et al., Scalable-manufactured randomized glass-polymer hybrid metamaterial for daytime radiative cooling, *Science* 355 (2017) 1062–1066, <https://doi.org/10.1126/science.aai7899>.
- [23] K. Sun, C.A. Riedel, Y. Wang, A. Urbani, M. Simeoni, S. Mengali, et al., Metasurface Optical Solar Reflectors Using AZO Transparent Conducting Oxides for Radiative Cooling of Spacecraft, *ACS Photonics* 5 (2017) 495–501, <https://doi.org/10.1021/acspophotonics.7b00991>.
- [24] J. Wang, G. Tan, R. Yang, D. Zhao, Materials, structures, and devices for dynamic radiative cooling, *Cell Reports Physical Science* 3 (2022), <https://doi.org/10.1016/j.xcrp.2022.101198>.
- [25] Y. An, Y. Fu, J.-G. Dai, X. Yin, D. Lei, Switchable radiative cooling technologies for smart thermal management, *Cell Reports Physical Science* 3 (2022), <https://doi.org/10.1016/j.xcrp.2022.101098>.
- [26] Z. Xia, Z. Fang, Z. Zhang, K. Shi, Z. Meng, Easy Way to Achieve Self-Adaptive Cooling of Passive Radiative Materials, *ACS Appl. Mater. Interfaces* 12 (2020) 27241–27248, <https://doi.org/10.1021/acsami.0c05803>.
- [27] M. Ono, K. Chen, W. Li, S. Fan, Self-adaptive radiative cooling based on phase change materials, *Opt. Express* 26 (2018) A777–A787, <https://doi.org/10.1364/OE.26.00A777>.
- [28] S.R. Wu, K.L. Lai, C.M. Wang, Passive temperature control based on a phase change metasurface, *Sci. Rep.* 8 (2018) 7684, <https://doi.org/10.1038/s41598-018-26150-9>.
- [29] D. Chae, M. Kim, P.-H. Jung, S. Son, J. Seo, Y. Liu, et al., Spectrally Selective Inorganic-Based Multilayer Emitter for Daytime Radiative Cooling, *ACS Appl. Mater. Interfaces* 12 (2020) 8073–8081, <https://doi.org/10.1021/acsami.9b16742>.
- [30] C. Feng, P. Yang, H. Liu, M. Mao, Y. Liu, T. Xue, et al., Bilayer porous polymer for efficient passive building cooling, *Nano Energy* 85 (2021), 105971, <https://doi.org/10.1016/j.nanoen.2021.105971>.
- [31] Z. Cheng, H. Han, F. Wang, Y. Yan, X. Shi, H. Liang, et al., Efficient radiative cooling coating with biomimetic human skin wrinkle structure, *Nano Energy* 89 (2021), 106377, <https://doi.org/10.1016/j.nanoen.2021.106377>.
- [32] H. Zhong, Y. Li, P. Zhang, S. Gao, B. Liu, Y. Wang, et al., Hierarchically Hollow Microfibers as a Scalable and Effective Thermal Insulating Cooler for Buildings, *ACS Nano* 15 (2021) 10076–10083, <https://doi.org/10.1021/acsnano.1c01814>.
- [33] Z. Chen, L. Zhu, A. Raman, S. Fan, Radiative cooling to deep sub-freezing temperatures through a 24-h day-night cycle, *Nat. Commun.* 7 (2016) 13729, <https://doi.org/10.1038/ncomms13729>.
- [34] H. Ma, K. Yao, S. Dou, M. Xiao, M. Dai, L. Wang, et al., Multilayered SiO₂/Si3N₄ photonic emitter to achieve high-performance all-day radiative cooling, *Sol. Energy Mater. Sol. Cells* 212 (2020), 110584, <https://doi.org/10.1016/j.solmat.2020.110584>.
- [35] D. Chae, H. Lim, S. So, S. Son, S. Ju, W. Kim, et al., Spectrally Selective Nanoparticle Mixture Coating for Passive Daytime Radiative Cooling, *ACS Appl. Mater. Interfaces* 13 (2021) 21119–21126, <https://doi.org/10.1021/acsami.0c20311>.
- [36] U. Banik, A. Agrawal, H. Meddeb, O. Sergeev, N. Reininghaus, M. Gotz-Kohler, et al., Efficient Thin Polymer Coating as a Selective Thermal Emitter for Passive Daytime Radiative Cooling, *ACS Appl. Mater. Interfaces* 13 (2021) 24130–24137, <https://doi.org/10.1021/acsami.1c04056>.
- [37] L. Zhou, H. Song, J. Liang, M. Singer, M. Zhou, E. Stegenburgs, et al., A polydimethylsiloxane-coated metal structure for all-day radiative cooling, *Nat. Sustainability* 2 (2019) 718–724, <https://doi.org/10.1038/s41893-019-0348-5>.
- [38] Y. Yang, L. Long, S. Meng, N. Denisuk, G. Chen, L. Wang, et al., Bulk material based selective infrared emitter for sub-ambient daytime radiative cooling, *Sol. Energy Mater. Sol. Cells* 211 (2020), 110548, <https://doi.org/10.1016/j.solmat.2020.110548>.
- [39] T. Wang, Y. Wu, L. Shi, X. Hu, M. Chen, L. Wu, A structural polymer for highly efficient all-day passive radiative cooling, *Nat. Commun.* 12 (2021) 365, <https://doi.org/10.1038/s41467-020-20646-7>.

- [40] Y. Weng, W. Zhang, Y. Jiang, W. Zhao, Y. Deng, Effective daytime radiative cooling via a template method based PDMS sponge emitter with synergistic thermo-optical activity, *Sol. Energy Mater. Sol. Cells* 230 (2021), 111205, <https://doi.org/10.1016/j.solmat.2021.111205>.
- [41] J. Liang, J. Wu, J. Guo, H. Li, X. Zhou, S. Liang, et al., Radiative cooling for passive thermal management towards sustainable carbon neutrality. *National Science, Review* 10 (2022), <https://doi.org/10.1093/nsr/nwac208>.
- [42] Y. Yang, Designing Porous Polymers for Daytime Radiative Cooling. *Video Proc. Adv. Mater.* 210149 (2021).
- [43] Y. Zhang, X. Tan, G. Qi, X. Yang, D. Hu, P. Fyffe, et al., Effective radiative cooling with ZrO₂/PDMS reflective coating, *Sol. Energy Mater. Sol. Cells* 229 (2021), 111129, <https://doi.org/10.1016/j.solmat.2021.111129>.
- [44] S. Atiganyanun, J.B. Plumley, S.J. Han, K. Hsu, J. Cytrynbaum, T.L. Peng, et al., Effective Radiative Cooling by Paint-Format Microsphere-Based Photonic Random Media, *ACS Photonics* 5 (2018) 1181–1187, <https://doi.org/10.1021/acsphtons.7b01492>.
- [45] X. Yu, J. Chan, C. Chen, Review of Radiative Cooling Materials: Performance Evaluation and Design Approaches, *Nano Energy* 88 (2021), 106259, <https://doi.org/10.1016/j.nanoen.2021.106259>.
- [46] J. Mandal, Y. Yang, N. Yu, A.P. Raman, Paints as a Scalable and Effective Radiative Cooling Technology for Buildings, *Joule*. 4 (2020) 1350–1356, <https://doi.org/10.1016/j.joule.2020.04.010>.
- [47] M. Santamouris, J. Feng, Recent Progress in Daytime Radiative Cooling: Is It the Air Conditioner of the Future? *Buildings* 8 (2018) 168, <https://doi.org/10.3390/buildings8120168>.
- [48] A.R. Gentle, G.B. Smith, Radiative heat pumping from the Earth using surface phonon resonant nanoparticles, *Nano Lett.* 10 (2010) 373–379, <https://doi.org/10.1021/nl903271d>.
- [49] X. Li, J. Peoples, P. Yao, X. Ruan, Ultrawhite BaSO₄ Paints and Films for Remarkable Daytime Subambient Radiative Cooling, *ACS Appl. Mater. Interfaces* 13 (2021) 21733–21739, <https://doi.org/10.1021/acsmami.1c02368>.
- [50] J.P. Bijarniya, J. Sarkar, P. Maiti, Performance simulation of polymer-based nanoparticle and void dispersed photonic structures for radiative cooling, *Sci. Rep.* 11 (2021) 893.
- [51] X. Sun, Y. Sun, Z. Zhou, M.A. Alam, P. Bermel, Radiative sky cooling: fundamental physics, materials, structures, and applications, *Nanophotonics*. 6 (2017) 997–1015, <https://doi.org/10.1515/nanoph-2017-0020>.
- [52] D. Li, X. Liu, W. Li, Z. Lin, B. Zhu, Z. Li, et al., Scalable and hierarchically designed polymer film as a selective thermal emitter for high-performance all-day radiative cooling, *Nat. Nanotechnol.* 16 (2021) 153–158, <https://doi.org/10.1038/s41565-020-0800-4>.
- [53] S. Zhong, L. Yi, J. Zhang, T. Xu, L. Xu, X. Zhang, et al., Self-cleaning and spectrally selective coating on cotton fabric for passive daytime radiative cooling, *Chem. Eng. J.* 407 (2021), 127104, <https://doi.org/10.1016/j.cej.2020.127104>.
- [54] D. Wu, C. Liu, Z. Xu, Y. Liu, Z. Yu, L. Yu, et al., The design of ultra-broadband selective near-perfect absorber based on photonic structures to achieve near-ideal daytime radiative cooling, *Mater. Des.* 139 (2018) 104–111, <https://doi.org/10.1016/j.matdes.2017.10.077>.
- [55] C. Zou, G. Ren, M.M. Hossain, S. Nirantar, W. Withayachumnankul, T. Ahmed, et al., Metal-Loaded Dielectric Resonator Metasurfaces for Radiative Cooling, *Adv. Opt. Mater.* 5 (2017) 1700460, <https://doi.org/10.1002/adom.201700460>.
- [56] T. Liu, J. Takahara, Ultrabroadband absorber based on single-sized embedded metal-dielectric-metal structures and application of radiative cooling, *Opt. Express* 25 (2017) A612–A627, <https://doi.org/10.1364/OE.25.00A612>.
- [57] Zhu L, Raman AP, Fan S. Radiative cooling of solar absorbers using a visibly transparent photonic crystal thermal blackbody. *Proceedings of the National Academy of Sciences of the United States of America.* 2015;112:12282-7. 10.1073/pnas.1509453112.
- [58] Q. Zhai, Q. Zhu, Radiative cooling film with self-cleaning function, *Sol. Energy Mater. Sol. Cells* 228 (2021), 111117, <https://doi.org/10.1016/j.solmat.2021.111117>.
- [59] S. Tao, X. Xu, M. Chen, W. Xu, L. Li, Z. Fang, et al., Construction of efficient passive radiative cooling emitter with selective emission in the whole atmospheric window and durable anti-contamination performance, *Sol. Energy Mater. Sol. Cells* 224 (2021), 110998, <https://doi.org/10.1016/j.solmat.2021.110998>.
- [60] R.A. Yalcin, E. Blandre, K. Joulain, J. Drévillon, Colored Radiative Cooling Coatings with Nanoparticles, *ACS Photonics* 7 (2020) 1312–1322, <https://doi.org/10.1021/acsphtons.0c00513>.
- [61] T. Suichi, A. Ishikawa, T. Tanaka, Y. Hayashi, K. Tsuruta, Whitish daytime radiative cooling using diffuse reflection of non-resonant silica nanoshells, *Sci. Rep.* 10 (2020) 6486, <https://doi.org/10.1038/s41598-020-63591-7>.
- [62] S.Y. Jeong, C.Y. Tso, Y.M. Wong, C.Y.H. Chao, B. Huang, Daytime passive radiative cooling by ultra emissive bio-inspired polymeric surface, *Sol. Energy Mater. Sol. Cells* 206 (2020), 110296, <https://doi.org/10.1016/j.solmat.2019.110296>.
- [63] S. Wang, Y. Wang, Y. Zou, G. Chen, J. Ouyang, D. Jia, et al., Biologically Inspired Scalable-Manufactured Dual-layer Coating with a Hierarchical Micropattern for Highly Efficient Passive Radiative Cooling and Robust Superhydrophobicity, *ACS Appl. Mater. Interfaces* 13 (2021) 21888–21897, <https://doi.org/10.1021/acsmami.1c05651>.
- [64] M. Chen, D. Pang, H. Yan, Colored passive daytime radiative cooling coatings based on dielectric and plasmonic spheres, *Appl. Therm. Eng.* (2022) 216, <https://doi.org/10.1016/j.applthermaleng.2022.119125>.
- [65] H. Bao, C. Yan, B. Wang, X. Fang, C.Y. Zhao, X. Ruan, Double-layer nanoparticle-based coatings for efficient terrestrial radiative cooling, *Sol. Energy Mater. Sol. Cells* 168 (2017) 78–84, <https://doi.org/10.1016/j.solmat.2017.04.020>.
- [66] J. Yang, X. Gao, Y. Wu, T. Zhang, H. Zeng, X. Li, Nanoporous silica microspheres-poly(methylpentene) (TPX) hybrid films toward effective daytime radiative cooling, *Sol. Energy Mater. Sol. Cells* 206 (2020), 110301, <https://doi.org/10.1016/j.solmat.2019.110301>.
- [67] Y. Liu, S. Son, D. Chae, P.-H. Jung, H. Lee, Acrylic membrane doped with Al₂O₃ nanoparticle resonators for zero-energy consuming radiative cooling, *Sol. Energy Mater. Sol. Cells* 213 (2020), 110561, <https://doi.org/10.1016/j.solmat.2020.110561>.
- [68] C. Lin, Y. Li, C. Chi, Y.S. Kwon, C.Y. Tso, C. Chao, et al., A Solution-processed Inorganic Emitter with High Spectral Effectiveness for E, *researchsquare*. 34 (2109350) (2021), <https://doi.org/10.21203/rs.3.rs-235967/v1>.
- [69] D. Lee, M. Go, S. Son, M. Kim, T. Badloe, H. Lee, et al., Sub-ambient daytime radiative cooling by silica-coated porous anodic aluminum oxide, *Nano Energy* 79 (2021), 105426, <https://doi.org/10.1016/j.nanoen.2020.105426>.
- [70] D. Chae, S. Son, H. Lim, P.H. Jung, J. Ha, H. Lee, Scalable and paint-format microparticle-polymer composite enabling high-performance daytime radiative cooling, *Materials Today Physics*. 18 (2021), 100389, <https://doi.org/10.1016/j.mtp.2021.100389>.
- [71] S. Liang, M. Wang, W. Gao, H. Diao, J. Luo, Recyclable, UV-Blocking, and Radiative Cooling Multifunctional Composite Membranes, *ACS Omega* (2022), <https://doi.org/10.1021/acsomega.2c02162>.
- [72] W. Huang, Y. Chen, Y. Luo, J. Mandal, W. Li, M. Chen, et al., Scalable Aqueous Processing-Based Passive Daytime Radiative Cooling Coatings, *Adv. Funct. Mater.* 31 (2021) 2010334, <https://doi.org/10.1002/adfm.202010334>.
- [73] K. Zhou, W. Li, B.B. Patel, R. Tao, Y. Chang, S. Fan, et al., Three-Dimensional Printable Nanoporous Polymer Matrix Composites for Daytime Radiative Cooling, *Nano Lett.* 21 (2021) 1493–1499, <https://doi.org/10.1021/acs.nanolett.0c04810>.
- [74] J. Zhang, Z. Zhou, H. Tang, J. Xing, J. Quan, J. Liu, et al., Mechanically Robust and Spectrally Selective Convection Shield for Daytime Subambient Radiative Cooling, *ACS Appl. Mater. Interfaces* 13 (2021) 14132–14140, <https://doi.org/10.1021/acsmami.0c21204>.
- [75] J. Zhang, Z. Zhou, J. Quan, D. Zhang, J. Sui, J. Yu, et al., A flexible film to block solar radiation for daytime radiative cooling, *Sol. Energy Materials and Solar Cells*. 225 (2021), 111029, <https://doi.org/10.1016/j.solmat.2021.111029>.
- [76] Z. Yang, H. Sun, Y. Xi, Y. Qi, Z. Mao, P. Wang, et al., Bio-inspired structure using random, three-dimensional pores in the polymeric matrix for daytime radiative cooling, *Sol. Energy Mater. Sol. Cells* 227 (2021), 111101, <https://doi.org/10.1016/j.solmat.2021.111101>.
- [77] B. Xiang, R. Zhang, Y. Luo, S. Zhang, L. Xu, H. Min, et al., 3D porous polymer film with designed pore architecture and auto-deposited SiO₂ for highly efficient passive radiative cooling, *Nano Energy* 81 (2021), 105600, <https://doi.org/10.1016/j.nanoen.2020.105600>.
- [78] Y. Tian, H. Shao, X. Liu, F. Chen, Y. Li, C. Tang, et al., Superhydrophobic and Recyclable Cellulose-Fiber-Based Composites for High-Efficiency Passive Radiative Cooling, *ACS Appl. Mater. Interfaces* 13 (2021) 22521–22530, <https://doi.org/10.1021/acsmami.1c04046>.
- [79] Y. Tian, X. Liu, J. Li, A. Caratenuto, S. Zhou, Y. Deng, et al., Scalable, fire-retardant, and spectrally robust melamine-formaldehyde photonic bulk for efficient daytime radiative cooling, *Appl. Mater. Today* 24 (2021), 101103, <https://doi.org/10.1016/j.apmt.2021.101103>.
- [80] J.K. Pradhan, D. Pratap, S.A. Ramakrishna, Thin nanoporous anodic alumina film on aluminium for passive radiative cooling, *Pramana* 95 (2021) 46, <https://doi.org/10.1007/s12043-021-02076-2>.
- [81] W. Gao, Z. Lei, K. Wu, Y. Chen, Reconfigurable and Renewable Nano-Micro-Structured Plastics for Radiative Cooling, *Adv. Funct. Mater.* 31 (2021) 2100535, <https://doi.org/10.1002/adfm.202100535>.
- [82] X. Chen, M. He, S. Feng, Z. Xu, H. Peng, S. Shi, et al., Cellulose-based porous polymer film with auto-deposited TiO₂ as spectrally selective materials for passive daytime radiative cooling, *Opt. Mater.* 120 (2021), 111431, <https://doi.org/10.1016/j.optmat.2021.111431>.
- [83] S. Son, Y. Liu, D. Chae, H. Lee, Cross-Linked Porous Polymeric Coating without a Metal-Reflective Layer for Sub-Ambient Radiative Cooling, *ACS Appl. Mater. Interfaces* 12 (2020) 57832–57839, <https://doi.org/10.1021/acsmami.0c14792>.
- [84] F.I. Chowdhury, Q. Xu, K. Sinha, X. Wang, Novel application of lignin biopolymer for radiative cooling, *Infrared Phys. Technol.* 117 (2021), 103840, <https://doi.org/10.1016/j.infrared.2021.103840>.
- [85] W. Jing, S. Zhang, W. Zhang, Z. Chen, C. Zhang, D. Wu, et al., Scalable and Flexible Electrospun Film for Daytime Subambient Radiative Cooling, *ACS Appl. Mater. Interfaces* 13 (2021) 29558–29566, <https://doi.org/10.1021/acsmami.0c05364>.
- [86] Y. Chen, B. Dang, J. Fu, C. Wang, C. Li, Q. Sun, et al., Cellulose-Based Hybrid Structural Material for Radiative Cooling, *Nano Lett.* 21 (2021) 397–404, <https://doi.org/10.1021/acs.nanolett.0c03738>.
- [87] A. Hervé, J. Drévillon, Y. Ezzahri, K. Joulain, Radiative cooling by tailoring surfaces with microstructures: Association of a grating and a multi-layer structure, *J. Quant. Spectrosc. Radiat. Transf.* 221 (2018) 155–163, <https://doi.org/10.1016/j.jqsrt.2018.09.015>.
- [88] J. Liu, H. Tang, C. Jiang, S. Wu, L. Ye, D. Zhao, et al., Micro-Nano Porous Structure for Efficient Daytime Radiative Sky Cooling, *Adv. Funct. Mater.* 32 (2022) 2206962, <https://doi.org/10.1002/adfm.202206962>.

- [89] J. Zhang, J. Yuan, J. Liu, Z. Zhou, J. Sui, J. Xing, et al., Cover shields for sub-ambient radiative cooling: A literature review, *Renew. Sustain. Energy Rev.* 143 (2021), 110959, <https://doi.org/10.1016/j.rser.2021.110959>.
- [90] S. Son, S. Jeon, D. Chae, S.Y. Lee, Y. Liu, H. Lim, et al., Colored emitters with silica-embedded perovskite nanocrystals for efficient daytime radiative cooling, *Nano Energy* 79 (2021), 105461, <https://doi.org/10.1016/j.nanoen.2020.105461>.
- [91] X. Li, B. Sun, C. Sui, A. Nandi, H. Fang, Y. Peng, et al., Integration of daytime radiative cooling and solar heating for year-round energy saving in buildings, *Nat. Commun.* 11 (2020) 6101, <https://doi.org/10.1038/s41467-020-19790-x>.
- [92] J.-H. Wang, C.-H. Xue, B.-Y. Liu, X.-J. Guo, L.-C. Hu, H.-D. Wang, et al., A Superhydrophobic Dual-Mode Film for Energy-Free Radiative Cooling and Solar Heating, *ACS Omega* 7 (2022) 15247–15257, <https://doi.org/10.1021/acsomega.2c01947>.
- [93] B. Dai, X. Li, T. Xu, X. Zhang, Radiative Cooling and Solar Heating Janus Films for Personal Thermal Management, *ACS Appl. Mater. Interfaces* 14 (2022) 18877–18883, <https://doi.org/10.1021/acsmi.2c01370>.
- [94] H. Luo, Y. Zhu, Z. Xu, Y. Hong, P. Ghosh, S. Kaur, et al., Outdoor Personal Thermal Management with Simultaneous Electricity Generation, *Nano Lett.* 21 (2021) 3879–3886, <https://doi.org/10.1021/acs.nanolett.1c00400>.
- [95] H. Fang, W. Xie, X. Li, K. Fan, Y.T. Lai, B. Sun, et al., A Triple-Mode Midinfrared Modulator for Radiative Heat Management of Objects with Various Emissivity, *Nano Lett.* 21 (2021) 4106–4114, <https://doi.org/10.1021/acs.nanolett.1c01147>.
- [96] Z. Li, Y. Zhai, Y. Wang, G.M. Wendland, X. Yin, J. Xiao, Harnessing Surface Wrinkling-Cracking Patterns for Tunable Optical Transmittance, *Adv. Opt. Mater.* 5 (2017) 1700425, <https://doi.org/10.1002/adom.201700425>.
- [97] Y. Liu, R. Liu, J. Qiu, S. Wang, 4D printing of thermal responsive structure for environmentally adaptive radiative cooling and heating, *Journal of Advanced Manufacturing and Processing*, 4 (2021) e10107.
- [98] Q. Zhang, Y. Lv, Y. Wang, S. Yu, C. Li, R. Ma, et al., Temperature-dependent dual-mode thermal management device with net zero energy for year-round energy saving, *Nat. Commun.* 13 (2022) 4874, <https://doi.org/10.1038/s41467-022-32528-1>.
- [99] D. Li, C. Zhou, Y. Meng, C. Chen, C. Yu, Y. Long, et al., Deformable Thermo-Responsive Smart Windows Based on a Shape Memory Polymer for Adaptive Solar Modulations, *ACS Appl. Mater. Interfaces* 13 (2021) 61196–61204, <https://doi.org/10.1021/acsmi.1c19273>.
- [100] X. Xiao, D. Kong, X. Qiu, W. Zhang, F. Zhang, L. Liu, et al., Shape-Memory Polymers with Adjustable High Glass Transition Temperatures, *Macromolecules* 48 (2015) 3582–3589, <https://doi.org/10.1021/acs.macromol.5b00654>.
- [101] F. Pilate, A. Toncheva, P. Dubois, J.-M. Raquez, Shape-memory polymers for multiple applications in the materials world, *Eur. Polym. J.* 80 (2016) 268–294, <https://doi.org/10.1016/j.eurpolymj.2016.05.004>.
- [102] Y. Zenghui, Z. Yaoming, Z. Xinrui, W. Tingmei, W. Qihua, Research Progress of High Temperature Shape Memory Polymers, *J. Funct. Polym.* 35 (314–27) (2022), <https://doi.org/10.14133/j.cnki.1008-9357.20211020001>.
- [103] W. Zha, Y. Zhu, B. Ma, J. Yu, P. Ghosh, M. Qiu, et al., Nonvolatile High-Contrast Whole Long-Wave Infrared Emissivity Switching Based on In3SbTe2, *ACS Photonics* (2022), <https://doi.org/10.1021/acspophotonics.0c00714>.
- [104] A. Hessler, S. Wahl, T. Leuteritz, A. Antonopoulos, C. Stergianou, C.F. Schon, et al., In3SbTe2 as a programmable nanophotonics material platform for the infrared, *Nat. Commun.* 12 (2021) 924, <https://doi.org/10.1038/s41467-021-21175-7>.
- [105] W.W. Zhang, H. Qi, A.T. Sun, Y.T. Ren, J.W. Shi, Periodic trapezoidal VO2-Ge multilayer absorber for dynamic radiative cooling, *Opt. Express* 28 (2020) 20609–20623, <https://doi.org/10.1364/OE.396171>.
- [106] R. Guo, L. Shan, Y. Wu, Y. Cai, R. Huang, H. Ma, et al., Phase-Change Materials for Intelligent Temperature Regulation, *Mater. Today Energy* 23 (2021), 100888, <https://doi.org/10.1016/j.mtener.2021.100888>.
- [107] J.B. Kana Kana, G. Vignaud, A. Gibaud, M. Maaza, Thermally driven sign switch of static dielectric constant of VO 2 thin film, *Opt. Mater.* 54 (2016) 165–169, <https://doi.org/10.1016/j.optmat.2016.02.032>.
- [108] S. Taylor, L. Long, R. McBurney, P. Sabbagh, J. Chao, L. Wang, Spectrally-selective vanadium dioxide based tunable metafilm emitter for dynamic radiative cooling, *Sol. Energy Mater. Sol. Cells* 217 (2020), 110739.
- [109] M. Kim, D. Lee, Y. Yang, J. Rho, Switchable diurnal radiative cooling by doped VO2, *Opto-Electronic Advances* 4 (2021) 200006, <https://doi.org/10.29026/oea.2021.200006>.
- [110] K. Tang, K. Dong, J. Li, M.P. Gordon, F.G. Reichertz, H. Kim, et al., Temperature-adaptive radiative coating for all-season household thermal regulation, *Science* 374 (2021) 1504–1509.
- [111] X. Ao, B. Li, B. Zhao, M. Hu, H. Ren, H. Yang, et al., Self-adaptive integration of photothermal and radiative cooling for continuous energy harvesting from the sun and outer space, *PNAS* 119 (2022), <https://doi.org/10.1073/pnas.2120557119>.
- [112] K. Araki, R.Z. Zhang, An optimized self-adaptive thermal radiation turn-down coating with vanadium dioxide nanowire array, *Int. J. Heat Mass Transf.* 191 (2022), <https://doi.org/10.1016/j.ijheatmasstransfer.2022.122835>.
- [113] W. Su, J. Darkwa, G. Kokogiannakis, Review of solid–liquid phase change materials and their encapsulation technologies, *Renew. Sustain. Energy Rev.* 48 (2015) 373–391, <https://doi.org/10.1016/j.rser.2015.04.044>.
- [114] M. Ono, M. Takata, M. Shirata, T. Yoshihiro, T. Tani, M. Naya, et al., Self-adaptive control of infrared emissivity in a solution-processed plasmonic structure, *Opt. Express* 29 (2021) 36048–36060, <https://doi.org/10.1364/OE.442462>.
- [115] Y. Meng, X. Li, S. Wang, C. Lau, H. Hu, Y. Ke, et al., Flexible smart photovoltaic foil for energy generation and conservation in buildings, *Nano Energy* 91 (2022), 106632, <https://doi.org/10.1016/j.nanoen.2021.106632>.
- [116] C. Ji, Z. Wu, L. Liu, X. Wu, J. Wang, X. Liu, et al., High thermochromic performance of Fe/Mg co-doped VO2 thin films for smart window applications, *J. Mater. Chem. C* 6 (2018) 6502–6509, <https://doi.org/10.1039/c8tc01111g>.
- [117] M. Liu, H.Y. Hwang, H. Tao, A.C. Strikwerda, K. Fan, G.R. Keiser, et al., Terahertz-field-induced insulator-to-metal transition in vanadium dioxide metamaterial, *Nature* 487 (2012) 345–348, <https://doi.org/10.1038/nature11231>.
- [118] F. Xu, X. Cao, Z. Shao, G. Sun, S. Long, T. Chang, et al., Highly Enhanced Thermochromic Performance of VO2 Film Using “Movable” Antireflective Coatings, *ACS Appl. Mater. Interfaces* 11 (2019) 4712–4718, <https://doi.org/10.1021/acsmi.8b20794>.
- [119] M. Kamalisarvestani, R. Saidur, S. Mekhilef, F.S. Javadi, Performance, materials and coating technologies of thermochromic thin films on smart windows, *Renew. Sustain. Energy Rev.* 26 (2013) 353–364, <https://doi.org/10.1016/j.rser.2013.05.038>.
- [120] H. Liu, H. Zong, L. Yan, D. Zhou, Y. Yin, G. Cao, et al., SnO2/VO2/SnO2 tri-layer thermochromic films with high luminous transmittance, remarkable solar modulation ability and excellent hydrophobicity grown on glass substrates, *Infrared Phys. Technol.* 113 (2021), 103648, <https://doi.org/10.1016/j.infrared.2021.103648>.
- [121] K. Sun, C. Wheeler, J.A. Hillier, S. Ye, I. Zeimpakis, A. Urbani, et al., Room Temperature Phase Transition of W-Doped VO2 by Atomic Layer Deposition on 200 mm Si Wafers and Flexible Substrates, *Adv. Opt. Mater.* (2022), <https://doi.org/10.1002/adom.202201326>.
- [122] M.J. Miller, J. Wang, Multilayer ITO/VO 2 /TiO 2 thin films for control of solar and thermal spectra, *Sol. Energy Mater. Sol. Cells* 154 (2016) 88–93, <https://doi.org/10.1016/j.solmat.2016.04.044>.
- [123] J. Zheng, S. Bao, P. Jin, TiO2(R)/VO2(M)/TiO2(A) multilayer film as smart window: Combination of energy-saving, antifogging and self-cleaning functions, *Nano Energy* 11 (2015) 136–145, <https://doi.org/10.1016/j.nanoen.2014.09.023>.
- [124] C. Sol, M. Portnoi, T. Li, K.L. Gurunatha, J. Schlafer, S. Guldin, et al., High-Performance Planar Thin Film Thermochromic Window via Dynamic Optical Impedance Matching, *ACS Appl. Mater. Interfaces* 12 (2020) 8140–8145, <https://doi.org/10.1021/acsmi.9b18920>.
- [125] D. Zhao, G. Zhang, X. Zhang, D. Li, Optical properties of paraffin at temperature range from 40 to 80 °C, *Optik* 157 (2018) 184–189, <https://doi.org/10.1016/j.ijleo.2017.11.093>.
- [126] E. Falahi, M. Barmar, K.M. Haghigheh, Preparation of phase-change material microcapsules with paraffin or camel fat cores: application to fabrics, *IRANIAN POLYMER JOURNAL (ENGLISH)*, 19 (2010) 277–286.
- [127] W. Su, P. Cai, R. Kang, L. Wang, G. Kokogiannakis, J. Chen, et al., Development of temperature-responsive transmission switch film (TRTSF) using phase change material for self-adaptive radiative cooling, *Appl. Energy* 322 (2022), 119457, <https://doi.org/10.1016/j.apenergy.2022.119457>.
- [128] F. Goia, Thermo-physical behaviour and energy performance assessment of PCM glazing system configurations: A numerical analysis, *Frontiers of Architectural Research*, 1 (2012) 341–347, <https://doi.org/10.1016/j.foar.2012.10.002>.
- [129] M.S. Kim, M.K. Kim, S.E. Jo, C. Joo, Y.J. Kim, Refraction-Assisted Solar Thermoelectric Generator based on Phase-Change Lens, *Sci. Rep.* 6 (2016) 27913, <https://doi.org/10.1038/srep27913>.
- [130] R. Yang, D. Li, S.L. Salazar, Z. Rao, M. Arici, W. Wei, Photothermal properties and photothermal conversion performance of nano-enhanced paraffin as a phase change thermal energy storage material, *Sol. Energy Mater. Sol. Cells* 219 (2021), 110792, <https://doi.org/10.1016/j.solmat.2020.110792>.
- [131] W.-D. Li, E.-Y. Ding, Preparation and characterization of cross-linking PEG/MDI/PE copolymer as solid-solid phase change heat storage material, *Sol. Energy Mater. Sol. Cells* 91 (2007) 764–768, <https://doi.org/10.1016/j.solmat.2007.01.011>.
- [132] P. Zhang, X. Xiao, Z.W. Ma, A review of the composite phase change materials: Fabrication, characterization, mathematical modeling and application to performance enhancement, *Appl. Energy* 165 (2016) 472–510, <https://doi.org/10.1016/j.apenergy.2015.12.043>.
- [133] Y. Shi, M. Hu, Y. Xing, Y. Li, Temperature-dependent thermal and mechanical properties of flexible functional PDMS/paraffin composites, *Mater. Des.* 185 (2020), 108219, <https://doi.org/10.1016/j.matdes.2019.108219>.
- [134] H.N. Apostoleris, M. Chiesa, M. Stefancich, Improved transparency switching in paraffin–PDMS composites, *J. Mater. Chem. C* 3 (2015) 1371–1377, <https://doi.org/10.1039/c4tc02546f>.
- [135] J. Zhang, G. Pu, M.R. Dubay, Y. Zhao, S.J. Severtson, Repositionable pressure-sensitive adhesive possessing thermal-stimuli switchable transparency, *J. Mater. Chem. C* 1 (2013) 1080–1086, <https://doi.org/10.1039/c2tc00471b>.
- [136] W. Su, R. Kang, P. Cai, M. Hu, G. Kokogiannakis, J. Darkwa, et al., Development of spectrally self-switchable cover with phase change material for dynamic radiative cooling, *Sol. Energy Mater. Sol. Cells* 251 (2023), <https://doi.org/10.1016/j.solmat.2022.112125>.
- [137] Y. Ke, J. Chen, G. Lin, S. Wang, Y. Zhou, J. Yin, et al., Smart windows: electro-, thermo-, mechano-, photochromic, and beyond, *Adv. Energy Mater.* 9 (2019) 1902066.
- [138] W. Xi, Y. Liu, W. Zhao, R. Hu, X. Luo, Colored radiative cooling: How to balance color display and radiative cooling performance, *Int. J. Therm. Sci.* 170 (2021), 107172, <https://doi.org/10.1016/j.ijthermalsci.2021.107172>.
- [139] Y. Ke, C. Zhou, Y. Zhou, S. Wang, S.H. Chan, Y. Long, Emerging Thermal-Responsive Materials and Integrated Techniques Targeting the Energy-Efficient

- Smart Window Application, *Adv. Funct. Mater.* 28 (2018) 1800113, <https://doi.org/10.1002/adfm.201800113>.
- [140] S. Wang, Y. Zhou, T. Jiang, R. Yang, G. Tan, Y. Long, Thermochromic smart windows with highly regulated radiative cooling and solar transmission, *Nano Energy* 89 (2021), 106440, <https://doi.org/10.1016/j.nanoen.2021.106440>.
- [141] X. Mei, T. Wang, M. Chen, L. Wu, A self-adaptive film for passive radiative cooling and solar heating regulation, *J. Mater. Chem. A* 10 (2022) 11092–11100, <https://doi.org/10.1039/D2TA01291J>.
- [142] X.-H. Li, C. Liu, S.-P. Feng, N.X. Fang, Broadband Light Management with Thermochromic Hydrogel Microparticles for Smart Windows, *Joule*. 3 (2019) 290–302, <https://doi.org/10.1016/j.joule.2018.10.019>.
- [143] Y. Zhou, S. Wang, J. Peng, Y. Tan, C. Li, F.Y.C. Boey, et al., Liquid Thermo-Responsive Smart Window Derived from Hydrogel, *Joule*. 4 (2020) 2458–2474, <https://doi.org/10.1016/j.joule.2020.09.001>.
- [144] C. Zhang, J. Yang, Y. Li, J. Song, J. Guo, Y. Fang, et al., Vapor-Liquid Transition-Based Broadband Light Modulation for Self-Adaptive Thermal Management, *Adv. Funct. Mater.* (2022), <https://doi.org/10.1002/adfm.202208144>.
- [145] H. Cho, J. Kwon, I. Ha, J. Jung, Y. Rho, H. Lee, et al., Mechano-thermo-chromic device with supersaturated salt hydrate crystal phase change. *Science, Advances* (2019;5:eaaav4916.), <https://doi.org/10.1126/sciadv.aav4916>.
- [146] E.P.A. van Heeswijk, J.J.H. Kloos, N. Grossiord, A.P.H.J. Schenning, Humidity-gated, temperature-responsive photonic infrared reflective broadband coatings, *J. Mater. Chem. A* 7 (2019) 6113–6119, <https://doi.org/10.1039/c9ta00993k>.
- [147] S.S. Lee, H.J. Seo, Y.H. Kim, S.H. Kim, Structural Color Palettes of Core-Shell Photonic Ink Capsules Containing Cholesteric Liquid Crystals, *Adv. Mater.* 29 (2017), <https://doi.org/10.1002/adma.201606894>.